Department of Civil Engineering

Assessment of air void content of asphalt using dielectric constant measurements by GPR and with microwave radar

Terhi Pellinen, Pekka Eskelinen,
Ari Hartikainen, Eeva Huuskonen-Snicker,
Jussi Eskelinen

Aalto University | SCIENCE + TECHNOLOGY | REPORT

Aalto University publication series
SCIENCE + **TECHNOLOGY** 8/2016

Assessment of air void content of asphalt using dielectric constant measurements by GPR and with microwave radar

Terhi Pellinen
Pekka Eskelinen
Ari Hartikainen
Eeva Huuskonen-Snicker
Jussi Eskelinen

Aalto University
School of Engineering
Department of Civil Engineering
Mineral based materials

Aalto University publication series
SCIENCE + **TECHNOLOGY** 8/2016

ISBN 978-952-60-6879-4 (pdf)
ISSN-L 1799-4896
ISSN 1799-4896 (printed)
ISSN 1799-490X (pdf)
http://urn.fi/URN:ISBN:978-952-60-6879-4

Unigrafia Oy
Helsinki 2016

Finland

Author

Author(s):Terhi Pellinen, Pekka Eskelinen, Ari Hartikainen, Eeva Huuskonen-Snicker, Jussi Eskelinen

Name of the publication

Assessment of air void content of asphalt using dielectric constant measurements by GPR and with microwave radar

Publisher School of Engineering

Unit Department of Civil Engineering

Series Aalto University publication series SCIENCE + TECHNOLOGY 8/2016

Field of research Highway Engineering

Abstract

In this report, we have presented microwave radar and GPR measurements as well as laboratory tests conducted in 2014-2016. The microwave radar was tested in three different construction sites. In addition, GPR measurements were obtained for comparison. Laboratory tests included traditional density measurements and 7-17 GHz VNA scanning of drill cores obtained from the test sites. A new laboratory measurement method using cavity resonator principle was introduced with promising results. Testing of this new method will be continued. The results indicate no clear correlation between air void content and GRP permittivity measurements. Permittivity is sensitive to the changes in the relative permittivity of aggregates and volume portions of aggregates and bitumen. The relative permittivity of the aggregates determines the base level for permittivity measured with radar or VNA. In the course of this research, it has become apparent that a new calibration procedure for the GPR measurements is needed. The aim in further research is to extract core samples from pavement areas with different densities to obtain a local calibration model.

Keywords asphalt, air voids, GPR, permittivity, calibration, dielectric constant

ISBN (printed)	**ISBN (pdf)** 978-952-60-6879-4	
ISSN-L 1799-4896	**ISSN (printed)** 1799-4896	**ISSN (pdf)** 1799-490X
Location of publisher Helsinki	**Location of printing** Helsinki	**Year** 2016
Pages 66	**urn** http://urn.fi/URN:ISBN:978-952-60-6879-4	

TABLE OF CONTENTS

GLOSSARY OF ACRONYMS 6
GLOSSARY OF SYMBOLS 7
FOREWORD 8
LAAJENNETTU TIIVISTELMÄ 9
1 INTRODUCTION 14
2 METHODS 15
2.1 Material dielectric permittivity 15
2.2 Microwave radar 15
2.3 Ground penetrating radar 16
2.4 Thermal camera 18
2.5 Density and air voids of asphalt core samples 18
2.6 Vector network analyzer scanner 19
2.7 Kernel density estimation 19
3 RESULTS OF LABORATORY AND FIELD STUDIES 20
3.1 Effective bulk permittivity of granules vs. solid effective permittivity 20
3.2 Kuopio test site 22
3.2.1 Density and air void content results 24
3.2.2 VNA scanning results 26
3.2.3 GPR results 26
3.2.4 Thermal camera results 27
3.2.5 Conclusions 29
3.3 Yläne test site 29
3.3.1 Density and air void results 31
3.3.2 VNA scanning results 34
3.3.3 Microwave radar results 35
3.3.4 GPR results 37
3.3.5 Conclusions 38
3.4 Hamina test site 39
3.4.1 Density and air void results 42
3.4.2 VNA scanning results 44
3.4.3 Microwave radar results 47
3.4.4 GPR results 49
3.4.5 Conclusions 51
3.5 Koskenkylä quarry reference measurements 51
3.5.1 Reference measurements results 52
3.5.2 Conclusions 56
3.6 Vt 3 and Vt 12 GPR repeat measurements 56
3.6.1 Drill core results from permittivity level jump in Vt 12 60
3.6.2 Conclusions 61
3.7 GPR results comparison 61
4 CONCLUDING REMARKS 65
5 REFERENCES 66

GLOSSARY OF ACRONYMS

AC	Asphalt Concrete
FTA	Finnish Transport Agency
GPR	Ground Penetrating Radar
MA	Mastic asphalt
QC/QA	Quality Control / Quality Assurance
SMA	Stone Mastic Asphalt
SSD	Saturated surface dry method
VFA/ VFB	Voids Filled with Bitumen
VMA	Voids in Mineral Aggregate
VNA	Vector Network Analyzer

GLOSSARY OF SYMBOLS

V_a	Air void content, (%)
A	Amplitude
P_b	Asphalt binder content, (%)
ρ_p	Bulk density
G_{mb}	Bulk specific gravity, see ρ_p
ε_r^*	Complex dielectric constant (also relative permittivity)
μ^*	Complex permeability
ρ	Density
ε_0	Dielectric constant of free space, $8{,}8541878 \ldots \cdot 10^{-12}\ F/m$
ε_r''	Dielectric constant, imaginary part
ε_r'	Dielectric constant, real part
A_0	Incident amplitude
ρ_m	Maximum density of loose mixture
G_{mm}	Maximum specific gravity, see ρ_m
A_r	Reflected amplitude

FOREWORD

This report presents findings from Phase II of the study on *Assessment of Asphalt Pavement Density* (Tiiveyden mittauksen ja arvioinnin kehittäminen) included in the *Pavement Life Cycle Research Program, 2013-2017* (Elinkaaritehokas tiepäällyste, 2013-2017) commissioned by the Finnish Transport Agency (FTA). The FTA program officer is Pavement Engineer, Katri Eskola, and from Aalto University, the PI of the project is Prof. Terhi Pellinen. The research is a collaboration between the Civil Engineering Department and the Department of Electrical Engineering and Automation, where Prof. Pekka Eskelinen is in charge of electromagnetic measurements and research. Doctoral students, Eeva Huuskonen-Snicker and Ari Hartikainen have contributed to the analysis of the VNA and GPR data as well as to the preparation of this report. The authors wish to thank undergraduate student, Jussi Eskelinen, for his help in finalizing the report.

LAAJENNETTU TIIVISTELMÄ

Tässä raportissa kuvataan kaupallisten maatutkamittausten ja Aalto-yliopiston Sähkötekniikan laitoksen rakentaman mikroaaltotaajuustutkan kenttämittausten tulokset. Koekohteet olivat liikenteen alla olevilla maanteillä sekä uudisrakennuskohteessa Vt 7:llä. Lisäksi raportissa esitetään koekohteista otettujen porapalojen dielektrisyysmittausten tulokset sekä verifioidaan asfaltin raaka-aineiden permittiivisyysmittausten tuloksia.

- Kuopio koealue Vt 5, mitattu kesällä 2014
- Yläne koeosuus Mt 210, mitattu kesällä 2014
- Hamina uudisrakennus koeosuus Vt 7, mitattu kesällä 2014
- Koskenkylä murskaamon koealue, mitattu kesällä 2015
- Tampere Vt 3 and Vt 12 koeosuudet, mitattu uudelleen syksyllä 2015

Seuraavassa esitetään lyhyt yhteenveto ja keskeiset johtopäätökset sekä näiden perusteella annetut suositukset. Suositukset koskevat päällysteen tiiveyden maatutkamittausmenetelmän tarkennusta (1-2 GHz GPR-laitteet) sekä asfalttipäällysteen paksuuden mittaamista ko. laitteilla.

Tutkamittauksen virhelähteet ε_r' arvossa

Kuvassa Figure 38 (s. 56) on esitetty esimerkki tieosasta, jossa ε_r' arvo on mitattu aikasarjana. Virhelähteet mitatun parametrin arvossa voivat tutkimusten mukaan olla esimerkiksi:

- tutkan laitetekninen kalibrointi ja kalibroinnin pysyvyys
- heijasteet alapuolisesta rakenteesta (taajuus) ja pulssin pituus
- vesi huokostilassa (mittausajankohta)
- signaalin maksimiamplitudin heijasteen valinta (mittauksen tulkinta)

Virhelähteet ε_r' arvon kalibroinnissa tyhjätilaksi

- Päällysteessä on vettä ja saatu ε_r' arvo on suurempi kuin fysikaalisesti kuivalle päällysteelle on mahdollista (massan maksimitiheys)
- Kun päällysteessä on vettä, PANK-kalibrointiyhtälö (PANK-4122) häivyttää suuret tyhjätilat ja tyhjätilan hajonta vääristyy, samoin keskimääräinen tyhjätila jää todellista alhaisemmaksi
- Käytetty kappaletiheyden mittausmenetelmä laboratoriossa vääristää todellista tyhjätilaa jos näyte on ohut ja siinä on reikiä. Tämä ongelma on havaittu esim. hyvin ohuiden Remix-pintausten kohdalla.
- Tutka mittaa tyhjätilaa absoluuttisesti, kun taas laboratoriomenetelmät ovat suhteellisia (massakohtaisia) ja käsittelevät mm. näytteen pintahuokosia eri tavalla.

Mahdollisia muutoksia ja tarkennuksia tutkamittausmenetelmään tiiveyden mittaamiseksi

- Dielektrisyyden ε_r' hajonnalle raja-arvot
    - Kesän 2016 aikana seurataan hajontoja ja kerätään mittausdataa analysointia varten.

    - Alustava teoreettinen arvio on että n. 0.11 keskihajonta ε_r' arvossa (kuiva päällyste) on riittävän pieni, jotta tyhjätilan vaihtelu on varmasti sallituissa rajoissa. Esimerkkejä mittausten hajontojen muutoksista on annettu taulukossa Table 12 s. 59.
    - Näyttäisi, että hajonnat kuivassa ja märässä päällysteessä eivät ole yhteismitallisia koska veden dielektrisyys ε_r' vaihtelee 42-81 välillä ja ilman dielektrisyys on 1.
    - Hajontojen sallitut vaihtelut tulee siten skaalata päällysteen kosteuspitoisuuden perusteella.
- Uusi tiekohtainen kalibrointimalli tyhjätilalle porapalojen avulla
    - PANK-mallin asemasta käytetään porapaloista sovitettua mallia tiekohtaisesti
- Mittauksen ajankohdan rajoitukset tai suositukset aikaikkunana 2 viikkoa työn tekemisestä, ei kuitenkaan ennen kahta päivää päällystämisestä.
    - Paras ajankohta on noin viikko työn tekemisestä (veden vaikutuksen minimointi).
    - Myös kantavassa kerroksessa oleva vesi vaikuttaa tuloksiin ja vaikka päällyste olisi pintakuiva sateen jälkeen, kantavan kerroksen kosteus voi olla suurta.
- Päällysteen tiheyden laboratorio-mittausmenetelmän muutos SMA massalle: Parafilm-menetelmä SSD:n asemasta. Kokeillaan kesällä 2016 Parafilm-menetelmän käyttöä SMA massoille.
- Porapalojen otolle uudet ohjeet.
    - Otetaan palat tiiviistä ja harvasta kohdasta ja vähintään 3 porapalaa (mallinnus).
- Pilotoidaan porapalojen tarkempaa tutkimista: ρ_p, ρ_m, uutto: P_b ja rakeisuus, kiviaineseoksen tiheys ρ_k.
    - Lasketaan V_a, VMA, VFB ja verrataan massan suunnitteluarvoihin.
- Raportoinnille uudet ohjeet.
- Tutkan kalibrointi metallilevyllä ennen ja jälkeen kunkin mittausosuuden.

<u>Uusi tiekohtainen kalibrointimalli korvaamaan PANK-4122 kalibraatioyhtälöä</u>

Tutkimustiedon perusteella näyttäisi, että lineaarinen malli kuvaa dielektrisyyden ja tiheyden suhdetta parhaiten, mutta mallin sovitusta voi joutua tarkentamaan massan rakeisuuden perusteella. Uudessa menetelmässä otetaan ainakin kolme porapalaa, joihin malli sovitetaan: tiiviistä päällysteestä, joka edustaa kuormaväliä ja harvasta päällysteestä, joka edustaa kuormakatkoa. Kolmas porapala otetaan keskimääräisen näköisestä päällysteestä. Jos dielektrisyys kasvaa tyhjätilan kasvaessa, päällysteessä on luultavasti vettä. Veden vaikutus on kyettävä ottamaan huomioon mallinnuksessa. Mallin avulla lasketaan ε_r' arvoista tyhjätilat ja hajonnat.

Porapalojen tyhjätilat tutkitaan mittaamalla päällysteen tiheys SFS-EN 12697-6 ja asfalttimassan tiheys menetelmällä SFS-EN 12697-5 (menettely B). AB:n ja ABS:n kappaletiheys määritetään menettelyllä A (kuiva menetelmä) ja SMA:n ja ABK:n kappaletiheys määritetään menettelyllä B (SSD) ja C (Parafilm) ja AA:n menettelyllä D.

Tyhjätilan hajontojen perusteella lasketaan tilastolliset poikkeamat. Jos poikkeamat ylittävät raja-arvot (jotka asetettaan alustavasti nykyisten raja-arvojen perusteella) ja osoittavat epähomogeenista ja liian avointa päällystettä, varmennetaan tulos ottamalla lisää porapaloja.

Raportointi päällysteen tiiveyden tutkamittauksista

- Ilmoitetaan tulkitun ε_r, keskiarvo ja hajonnat, on tärkeää erottaa kuiva ja märkä mittaus, hajonnat eivät ole yhteismitallisia ja tulosten jälkikäsittelyssä käytetyt parametrit ja asetusarvot (mm. RoadDoctor) ilmoitetaan yksityiskohtaisesti.
- Kuvassa Figure 2 ja yhtälössä (Eq. 2) on esitetty maatutkan mittauksen periaate ja signaali. Maksimiamplitudi tulee ilman erillistä syytä valita kuvan mukaisesti ja sitä ei saa vaihtaa kesken mittauksen tulkinnan. Jos tästä poiketaan, se on ilmoitettava.
- Tie jaetaan samanlaisiin osiin ja jos keskimääräinen ε_r -taso selkeästi nousee tai laskee yli 50 metrin matkalle laskettuna kesken mittausjakson (esimerkki ongelmasta kuvassa Figure 41 s. 58), hajonnat lasketaan ko. tieosuuksille erikseen (kuiva mittaus).
- Tilastomatemaattiset poikkeamat lasketaan ja ilmoitetaan.
- Porapalat: kerrospaksuudet, ρ_p, ρ_m, (P_b ja rakeisuus, kiviaineseoksen tiheys ρ_k) sekä vastaavat dielektrisyyden arvot kalibrointia varten.
- Esitetään massan suunnittelu eli suhteitustiedot; sideainepitoisuus, massan tiheys, päällysteen tiheys VMA, VFB, tyhjätila, kiviaineksen seostiheys, tai yksittäisten kiviainesfraktioiden tiheydet, uuden kiviaineksen alkuperä, sekä fillerikiviaineksen alkuperä.

Ohuen asfalttikerroksen paksuuden mittaaminen kaupallisella maaperätutkalla (GPR)

Useimmat Suomessa tiemittauksiin käytettävät maaperätutkat (GPR) toimivat joko 1 GHz tai 2 GHz taajuusalueella. Tunnettujen kaupallisten laitteiden (esimerkiksi GSSI:n SIR 30) radio-osien tuottama pulssinpituus on likimain 1 ns. Edellä mainitut parametrit ovat aikanaan määräytyneet GPR-laitteiden alkuperäisen käyttötarkoituksen mukaan ja ne sopivat esimerkiksi metriluokan maakerrosten tutkimiseen, koska signaalin vaimennus on pieni 1-2 GHz alueella eikä syvyyserottelun tarvitse olla erityisen hyvä.

Jos GPR-laitteilla yritetään määritellä asfalttikerroksen paksuutta, ei 1 ns pulssilla voida edes teoriassa saavuttaa yksikäsitteistä varmuutta, mikäli yksittäinen asfaltin kerrospaksuus on 5 cm luokkaa (Suomessa usein pienempikin) ja alapuolisten rakenteiden sähköiset ominaisuudet vaihtelevat tuntemattomalla tavalla. Tämä johtuu siitä, että syvemmältä tulevat heijastukset ehtivät summautua mielivaltaisessa vaiheessa alkuperäiseen haluttuun rajapintasignaaliin ja ääritapauksessa voivat jopa ”hävittää” halutun rajapinnan tutkan signaalinkäsittelyn kannalta näkymättömiin. Koska 1 tai 2 GHz nimellistaajuinen sähkömagneettinen kenttä ei juurikaan vaimene 20-30 cm matkalla asfaltissa, väärien heijastusten todellista amplitudia ei tunneta. Mittauksen kannalta kohtalokas kerrosrakenne voi tietenkin olla peräisin varsinaisista asfalttitöistä, ehkä eri aikoina tehdyistä, mutta pelkkä tuntematon ja mittauskohdan mukaan vaihteleva, tien pinnalta näkymätön kantavan rakenteen vesipitoisuus riittää aiheuttamaan vastaavan ongelman, mikäli varsinaisia asfalttikerroksia on vain yksi.

Sekä 1 GHz että 2 GHz GPR-laitteiden perusongelma on riittämätön radio-osien (ml. antennit) kaistaleveys, joka ei mahdollista lyhempien pulssien käyttämistä. Ongelmaa ei voida poistaa tulosten matemaattisella jälkikäsittelyllä. Luotettava ohuiden asfalttikerrosten mittaus edellyttäisi, että tutkan radio-osat (lähetin, vastaanotin ja antennit) pystyvät käsittelemään 100-300 ps pulsseja.

Maasto-olosuhteisiin soveltuvia tämän vaatimuksen täyttäviä laitteita ei tiettävästi ole kaupallisesti vielä saatavilla.

Jos nykyisiä laitteita käytetään ohuiden asfalttikerrosten paksuuden mittaamiseen, on mittaustulosten silmämääräinen tulkinta ja tulkitsijan ammattitaito määräävässä asemassa tulosten oikeellisuuden kannalta. Manuaalinen signaalin tulkinta on kuitenkin aina altis virheille ja yksikäsitteistä varmuutta ei ole mahdollista saavuttaa. Tulkinnan virhemarginaalia voidaan tutkia esim. empiirisin vertailukokein ja aineiston ja tulkintatiedon lisääntyessä todennäköisyys virhepäätelmiin suppenee ko. mittausaineistolle ominaiselle keskimääräiselle tasolle.

1 INTRODUCTION

This report describes the results of Phase II of the *Assessment of Asphalt Pavement density* study funded by the Finnish Transport Agency. The objective of the study is to investigate if the existing GPR technique employed in Finland is sufficiently accurate to be used as a Quality Control/Quality Assurance (QC/QA) tool in assessing the compaction of newly laid asphalt pavements. The work consisted of field and laboratory experiments and a review of the existing PANK calibration method for the GPR measurements. The results for Phase I of the study are reported in Pellinen et al. 2015: *Assessment of air void content of asphalt using dielectric constant measurements by GPR and with VNA*, which is available in Aalto doc (http://urn.fi/URN:ISBN:978-952-60-6288-4).

Field experiments with the commercial GPRs and a self-made microwave radar were conducted in the summers of 2014 and 2015 on specific test roads and locations consisting of the following cases. In addition, follow-up measurements were conducted on highways Vt 3 and Vt 12, near the City of Tampere. Furthermore, raw materials collected from the quarry and the asphalt plant for Tampere test road were further studied and the results are reported here.

- Kuopio test road located on Vt 5, measured in the summer of 2014
- Yläne test road located on Mt 210, measured in the summer of 2014
- Hamina test road, new road construction on Vt 7, measured in the summer of 2014
- Koskenkylä quarry test site, measured in the summer of 2015
- Tampere test roads on Vt 3 and Vt 12, measured in the fall of 2015

Radar measurements and laboratory tests of pavement density were then compared with the Vector Network Analyzer (VNA) measurements conducted in the laboratory of Electrical Engineering at Aalto University. Vector network analysis is a method for accurately characterizing signal deformations by measuring their effect on the amplitude and phase of swept-frequency test signals.

The aim of the Kuopio, Yläne and Hamina test road measurements was to investigate the new microwave radar and compare it with the commercial GPR. Furthermore, a thermal camera was used during the laying of asphalt at Kuopio test site, but the microwave radar measurements failed due to hardware errors. Therefore, the measurements could not be compared.

The aim of the measurements at Koskenkylä quarry was to assess the commercial GPR and its depth resolution in a tightly controlled experiment with a known plastic reference material.

Vt 3 and Vt 12 measurements were conducted to verify the previously obtained results of the magnitude of permittivity values as a function of service time of a worn pavement surface.

2 METHODS

This section describes different measurement and data visualization techniques. Field studies included measurements with the microwave radar, operating at the 12-18 GHz frequency band, and Ground Penetrating Radar (GPR) measurements with a 1 GHz commercial pulse radar. Drilled core samples from the field tests were analyzed in the laboratory by measuring the bulk and maximum densities. In addition, some of the samples were scanned with a vector network analyzer (VNA) to obtain the dielectric permittivity distribution. It was possible to analyze thermal camera data from one of the field test locations.

2.1 Material dielectric permittivity

Dielectric permittivity ε^*, electrical conductivity σ, and magnetic permeability μ^* are material properties determining propagation and attenuation of the electromagnetic field. Permittivity ε^* is a complex variable

$$\varepsilon^* = \varepsilon_0 \varepsilon_r = \varepsilon_0(\varepsilon_r' + j\varepsilon_r''), \quad (1)$$

where ε_0 is the permittivity of free space, ε_r relative permittivity of material, ε_r' is the real part of relative permittivity and ε_r'' is the imaginary part of relative permittivity. The real part of frequency dependent relative permittivity describes the stored energy, whereas the imaginary part accounts for energy losses in the medium. In this study, we focus only on the real part of relative permittivity, which is determined by different methods for the asphalt pavement on the road or drilled samples in the laboratory. More about permittivity of materials can be found, for example, in Pellinen et al. (2015).

2.2 Microwave radar

Our previous report identified an insufficient depth resolution of commercial GPRs. Therefore, a new microwave radar was introduced, which utilizes the swept continuous wave principle. The sweep band is from 12 to 18 GHz and this sweep width allows for a depth resolution better than 10 mm. The microwave radar was tested on different pavements during the summers of 2014 and 2015. The initial construction of the radar system on a pulled cart (Figure 1 below on the left) is described in Olkkonen et al. (2014). For summer 2015, a microwave radar (Figure 1 below on the right) was mounted on a small radio-controlled four-wheel-drive rover (Huuskonen-Snicker et al. 2015).

Figure 1: *(On the left)* Microwave radar installed in a cart, and *(on the right)* the radio-controlled radar rover

The microwave radar system contains four microprocessors, and the data is processed on a laptop computer. The radar operates at zero intermediate frequency and the detected signal is obtained directly at the base band. Naturally, the benefit is a simple and low-cost design. Contrary to the more common in-phase/quadrature phase (I/Q) detection, the radar measures the reflected signal amplitude and the trigonometric cosine of its phase angle (compared to the transmitted signal). From these, the real part of permittivity is obtained with the help of a calibration signal from a material with known permittivity. Reflectivity calibration principles are explained in detail in Pellinen et al. (2015). A notable benefit of using a material with a known dielectric value, instead of the commonly used plain metal plate as the reference reflection source, is that this way a smaller dynamic range is required. The real pavement reflectivities yield signal magnitudes which are much closer to other materials, such as our plastic calibration material, than to the large aluminum alloy surface. The radar system can produce the ε_r' of the pavement with an uncertainty close to 0.1.

2.3 Ground penetrating radar

The commercial GPR devices used in evaluating air voids are commonly pulse radars with 1 or 2 GHz air horn antennas. They measure the amplitude and the delay time of the reflected waves. The dielectric value, in other words, the real part of relative permittivity, can in this case be calculated by using the Eq. (2).

$$\varepsilon_r = \left(\frac{1 + {A_r}/{A_0}}{1 - {A_r}/{A_0}} \right)^2 \tag{2}$$

where A_0 is the incident amplitude, A_r the reflected amplitude and ε_r the relative permittivity of asphalt. The incident amplitude is obtained from the calibration signal with a metal plate. The derivation of the Eq. (2) is shown in Pellinen et al. (2015), in addition to other information about

the GPR method. Figure 2 shows the definitions of pulse amplitude given by calibration method PANK-4122.

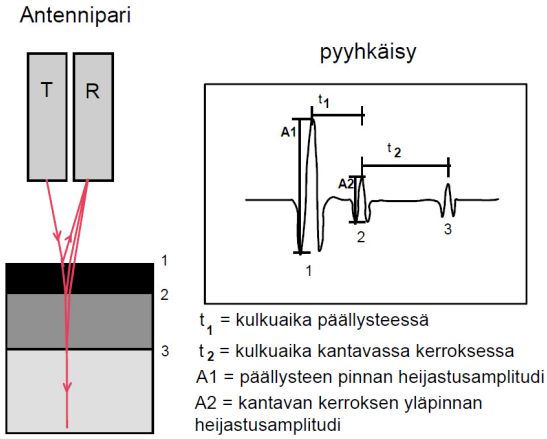

Figure 2: PANK-4122 calibration method. (T) is transmitting antenna and (R) is receiving antenna. Numbers 1, 2 and 3 describe different structural layers of road. No. 1 is the bound asphalt layer, 2 is the unbound base layer and 3 is the unbound subbase/subgrade layer

The incident and reflected amplitudes can be established in different ways. As shown in Figure 3, for a pulse radar, the peak-to-peak amplitude is obtained from the absolute difference between the negative and the positive peak. A GPR pulse signal consists of two negative peaks and one positive peak. The permittivity calculated with the first negative peak and the positive peaks is referred to as the permittivity from the first signal half. The permittivity calculated from the difference between the second negative peak and the positive peak is referred to as the permittivity from the second signal half. In the PANK-4122 calibration method, permittivity is calculated from the maximum difference between the negative and positive peaks. In this report, permittivities are calculated from the first signal half, unless stated otherwise.

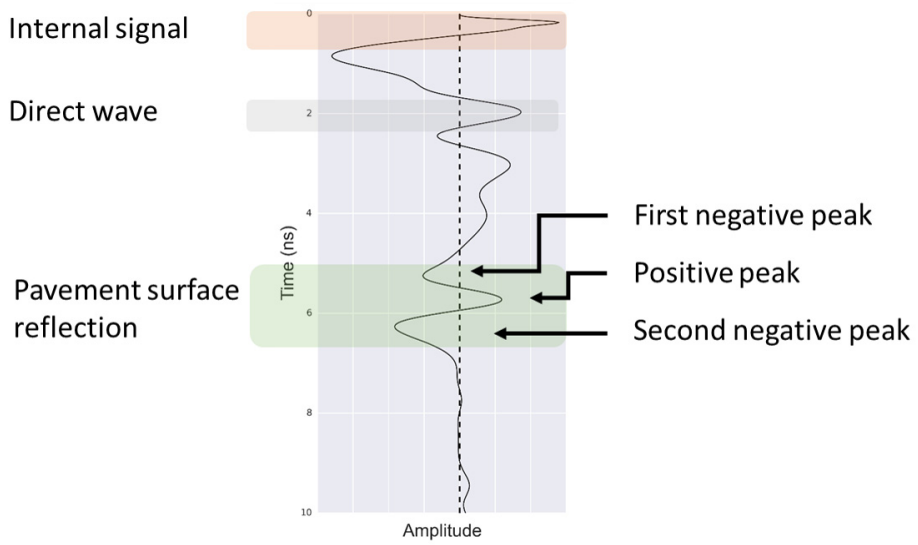

Figure 3: Determination of peak to peak components from GPR signal

2.4 Thermal camera

A thermal camera measures the infrared heat radiation energy which is presented as temperature. For the pavement construction application, the camera records the constructed pavement with a temperature record is captured perpendicularly at specific intervals across the constructed pavement and then saved. These captured lines are presented as temperature maps (see, for example, Figure 12). Thermal camera data can be used for the evaluation of asphalt mixture segregation (Nevalainen 2014).

2.5 Density and air voids of asphalt core samples

Several methods exist for obtaining the pavement density of asphalt depending on the asphalt mixture type. In water displacement methods, which are based on the Archimedes principle, specimen volume is calculated by weighing the specimen in a water bath and out of the water bath. The difference in weights is then converted to the volume of the specimen. The three methods that are used in SFS-EN 12967-8 for obtaining the density of the compacted asphalt sample are a dry method (no water in sample) (A); a saturated surface dry method (SSD) where water fills the asphalt air voids (B); a method based on the sample dimensions (D); and a method where the sample is sealed (C), for instance, wrapped with Parafilm. The dry method is used for dense mixtures, such as MA and AC, while the SSD is used for the SMA mixtures. Dimensions are not typically used for other than the porous asphalt (to be precise, open graded asphalt) as the large voids cannot be measured with other methods. In addition, obtaining density with core dimensions is not considered sufficiently accurate a method for the AC and SMA. The Parafilm method is not typically used as it is considered to be tedious. There are no limitations for water absorption in the SFS-EN 12967-8 method, but the equivalent AASHTO T-166 standard states that water absorption

should typically be below 2 percent. If more than 2 percent water by volume is absorbed by the sample, this method is deemed inappropriate.

The air void content of asphalt is derived from the pavement density. The air void content, V_a (%), is the ratio of the asphalt pavement density (ρ_p) and the maximum density (ρ_m),

$$V_a = \left(1 - \rho_p/\rho_m\right) \cdot 100. \quad (3)$$

2.6 Vector network analyzer scanner

Vector network analyzer (VNA) is a method of accurately measuring swept-frequency test signals, their amplitude, and phase delay. This work utilized two waveguide antennas that operate in the frequency band of 7-17 GHz in transmission configuration. In the transmission configuration, the antennas are on both sides of the sample. The footprint of the antennas is approximately a circle with a 20 mm diameter on the sample surface. The special scanner configuration was used in this study, which enables an automated moving of antennas with 5 mm steps in x- and y-directions. For most samples, ten-times-ten measurement points were measured. VNA measurements were conducted in the laboratory of Electrical Engineering at Aalto University. The VNA used in this research was the Wiltron 360 Network Analyzer.

Microwave frequencies of 7 to 17 GHz are used in laboratory studies because they enable a better depth resolution in the permittivity measurements. The additional advantage this provides is that the antenna size is smaller, which enables the measurement of pavement cores.

From the measured amplitude and phase, the real part of relative permittivity ε_r' can then be calculated by modified linear regression. However, the VNA recordings require some post-processing before the desired dielectric value is received. This calculation process is described in detail in Pellinen et al. (2015).

2.7 Kernel density estimation

The data visualization techniques used for this study include kernel density estimation (KDE) and violin plot, which is derived from the KDE. The KDE describes each sample point as a specified kernel, for example, a Gaussian kernel, and then sums kernels to produce the KDE. The kernel width can be set automatically with commonly used estimation rules or manually (Scott). When data was discretized, resulting in the automatic rules failing to represent underlying distribution, a manual kernel width was used in estimation. The commonly known histogram plot can be thought of as a discrete equivalent of the KDE plot.

The violin plot consists of a KDE plot that has been mirrored against its measurement axis. The violin plot can be thought of as a continuous analogy of a box plot. Usually, a violin plot includes a marker for the mean or the median value of the distribution.

3 RESULTS OF LABORATORY AND FIELD STUDIES

3.1 Effective bulk permittivity of granules vs. solid effective permittivity

Raw materials taken from test roads Vt 3 and Vt 12 are listed in our previous report (Pellinen et al. 2015). These materials were used to prepare raw material samples (Figure 4) for effective permittivity measurements with the VNA. To study further the effect of granularity on the bulk permittivity of asphalt, aggregate samples were measured and compared with the solid block of rock.

The aggregate blend sample (> 0.063 mm) was sieved from the cold feed aggregate blend sample by separating the filler fraction (< 0.063 mm) for the filler sample. This sieving of fines was undertaken to separate the mineralogy of the samples: the filler fraction was limestone and the rest of the aggregates were crushed from solid metavolcanic rock with intermediate composition (Samples 1 and 2). In addition, this separation of fines enabled an investigation of the effect of granularity on the bulk permittivity of material compared with the filler fraction.

All the effective bulk and solid permittivity results are presented in Table 1 and in Figure 5. Measurements were conducted using a VNA with variable scanning areas and a variable number of sample points (n). All results n (total) were within a reasonable range and no outliers were detected. During the measurement campaign, it became evident that the large aggregate particles caused multiple reflections and signal scattering, which artificially increased ε_r' and distorted the results.

The limestone filler sample had a low bulk permittivity (2.80) value and a very low standard deviation (0.08). This agrees with the high air void content (porosity) of the sample, which was measured by air and water tank method to be 62 %. Using a linear electromagnetic mixing model, the estimated permittivity would be 5.8 for the solid limestone. In comparison, for the aggregate blend ε_r' was 4.52 and the standard deviation was 0.94. This agrees with the measured porosity of the aggregate blend sample, which was 46 % on average. Therefore, the effective bulk permittivity of the aggregate blend was affected by the variation of the rock material itself, in other words, the mineralogy of solid rock (see the results of solid rock samples 1 and 2 shown in Table 1 and Figure 5), as well as the variation of aggregate size distribution and the amount of air voids (porosity) across the sample box.

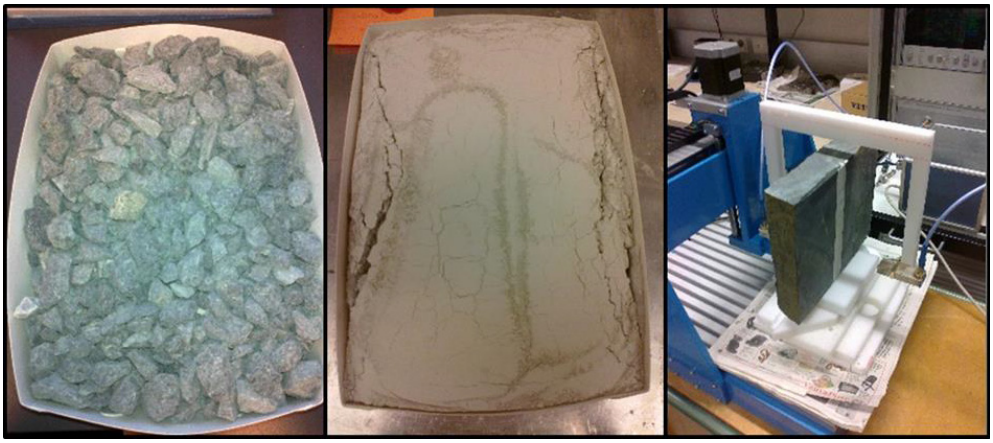

Figure 4: (*From left to right)* Aggregate blend sample, filler sample and rock slab 1 in VNA measurement

Table 1: Statistics of VNA measurements of raw materials from test roads Vt 3 and Vt 12

SAMPLE	**n (accepted)**	**n (total)**	**n (rejected)**	$\mathbf{mean}(\boldsymbol{\varepsilon_r})$	$\mathbf{std}(\boldsymbol{\varepsilon_r})$
Aggregate blend	100	100	0	4.52	0.94
Solid rock 1	900	900	0	6.23	0.27
Solid rock 2	225	225	0	5.85	0.29
Filler	100	100	0	2.80	0.08

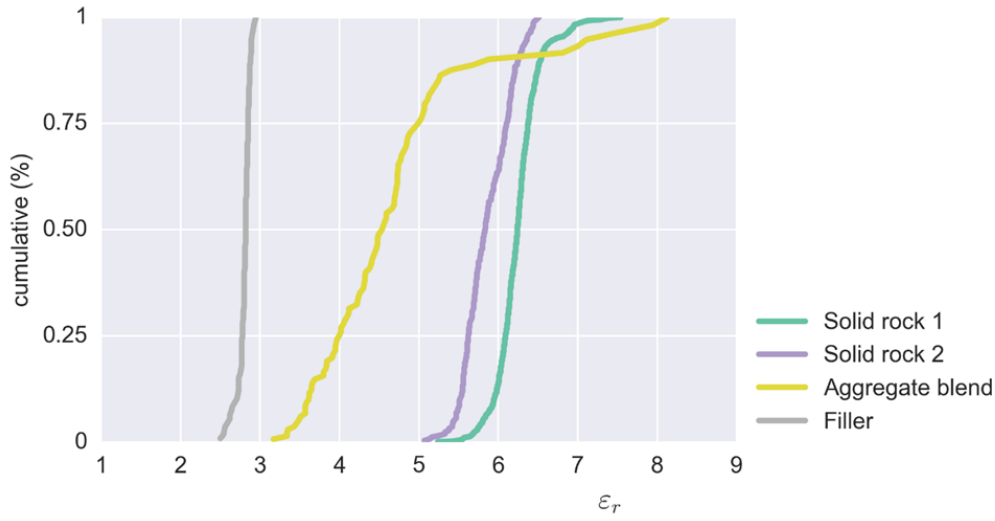

Figure 5: Cumulative distribution of VNA effective bulk and solid permittivity results of raw materials

3.2 Kuopio test site

In Kuopio, the aim was to compare two non-destructive testing methods, the microwave radar and thermal camera, to evaluate the newly laid asphalt wearing course. A section of highway was studied with different methods. Cored asphalt samples, with 150 mm core diameter, were extracted from the pavement for the laboratory analysis, shown in Figure 6. The Kuopio test site was located on Road 5, Lane 1 part 160.

Microwave radar measurements in Kuopio failed due to a hardware error. Therefore, the results could not be presented and analyzed.

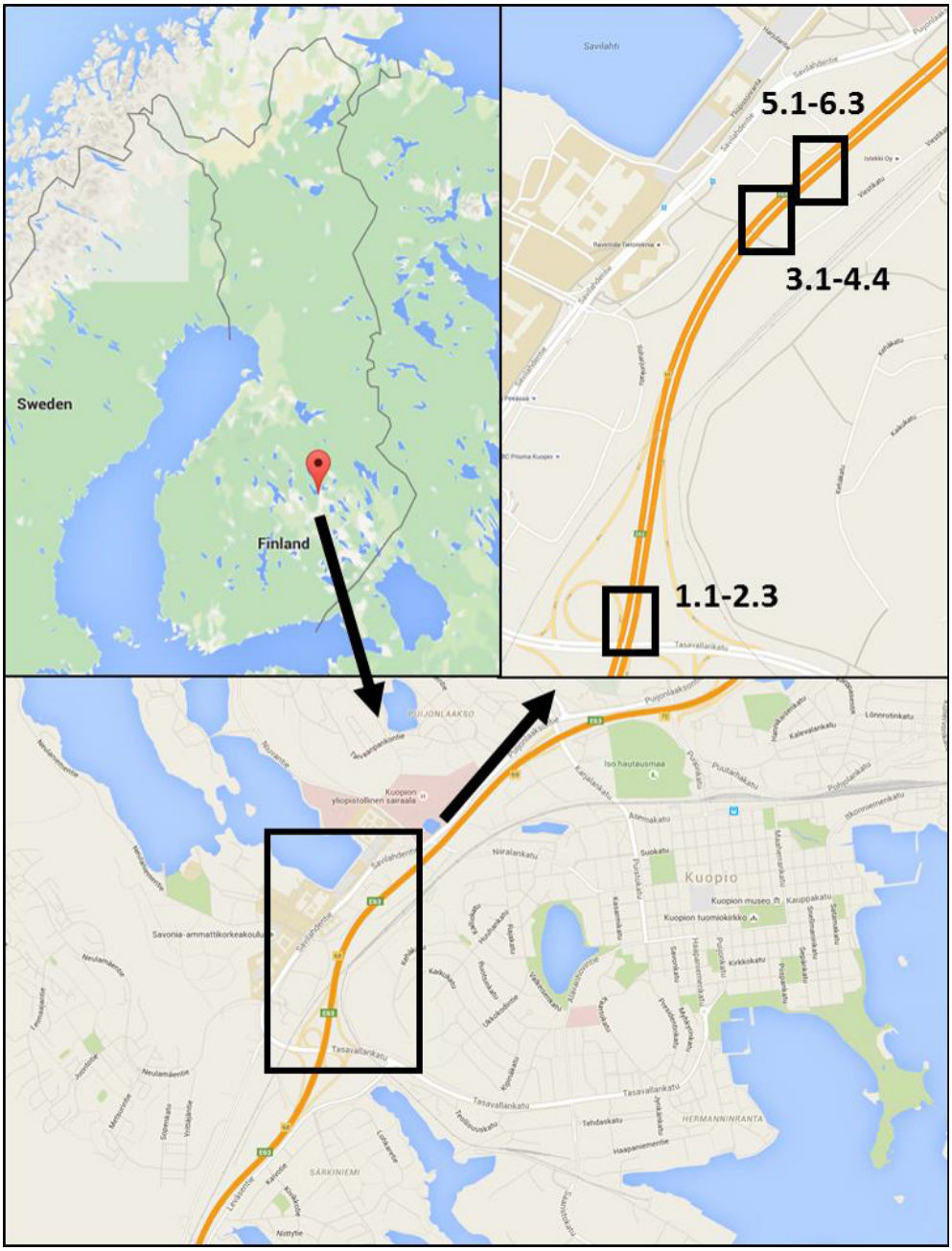

Figure 6: Map from Kuopio test site showing approximate drilling locations of asphalt samples (Map data ©2016 Google)

3.2.1 *Density and air void content results*

The bulk and maximum densities were measured in the laboratory according to (SFS-EN 12697-6 and SFS-EN 12697-5). Air voids were calculated based on the laboratory results, which are presented in Table 2 and Table 3. In Figure 7, air voids determined with different methods are compared for each sample. The laboratory results of Sample 4.1 are questionable as SSD and DRY produced values from 11.9 % to 4.5 %, respectively. In general, air void contents are rather high, the minimum being 4.1 %. Moreover, the maximum densities are high due to the high solid density of aggregates (Table 2). Sample 4.1 was extracted from the edge of the pavement, see Figure 12, which might explain its high air void content.

Table 2: Density and air void results of core samples from Kuopio

	G_{mb}				G_{mm}	V_a (%)			
SAMPLE	**SSD**	**DRY**	**DIM**	**PARAF.**		**SSD**	**DRY**	**DIM**	**PARAF.**
1.1	2.521	2.540	2.448	2.462	2.717	7.2	6.5	9.9	9.4
1.2	2.580	2.582	2.500	2.513	2.698	4.4	4.3	7.3	6.8
2.1	2.582	2.586	2.503	2.523	2.693	4.1	4.0	7.1	6.3
2.2	2.566	2.586	2.497	2.479	2.711	5.4	4.6	7.9	8.6
2.3	2.540	2.562	2.476	2.479	2.714	6.4	5.6	8.8	8.7
3.1	2.572	2.604	2.498	2.488	2.701	4.8	3.6	7.5	7.9
3.2	2.574	2.605	2.451	2.447	2.716	5.2	4.1	9.8	9.9
4.1	2.390	2.592	2.260	2.260	2.714	11.9	4.5	16.7	16.7
4.2	2.581	2.592	2.503	2.481	2.718	5.0	4.6	7.9	8.7
4.3	2.554	2.586	2.501	2.475	2.721	6.1	5.0	8.1	9.1
4.4	2.581	2.592	2.476	2.483	2.696	4.3	3.9	8.1	7.9
5.1	2.593	2.607	2.537	2.474	2.723	4.8	4.2	6.8	9.1
5.2	2.572	2.596	2.515	2.483	2.715	5.3	4.4	7.4	8.5
6.1	2.584	2.587	2.480	2.496	2.705	4.5	4.4	8.3	7.7
6.2	2.588	2.602	2.498	2.493	2.698	4.1	3.5	7.4	7.6
6.3	2.568	2.593	2.514	2.466	2.713	5.3	4.4	7.4	9.1
mean $_{total}$	2.558	2.588	2.477	2.467	2.710	5.6	4.5	8.5	8.9
std $_{total}$	0.049	0.017	0.063	0.059	0.010	1.9	0.7	2.4	2.3

Table 3: Solid density results of drill core samples from Kuopio

SAMPLE	SOLID DENSITY		
	< 0.125 mm	4-11.2 mm	11.2 mm >
3.1	2.834	3.010	3.017
4.3	2.856	3.028	3.025

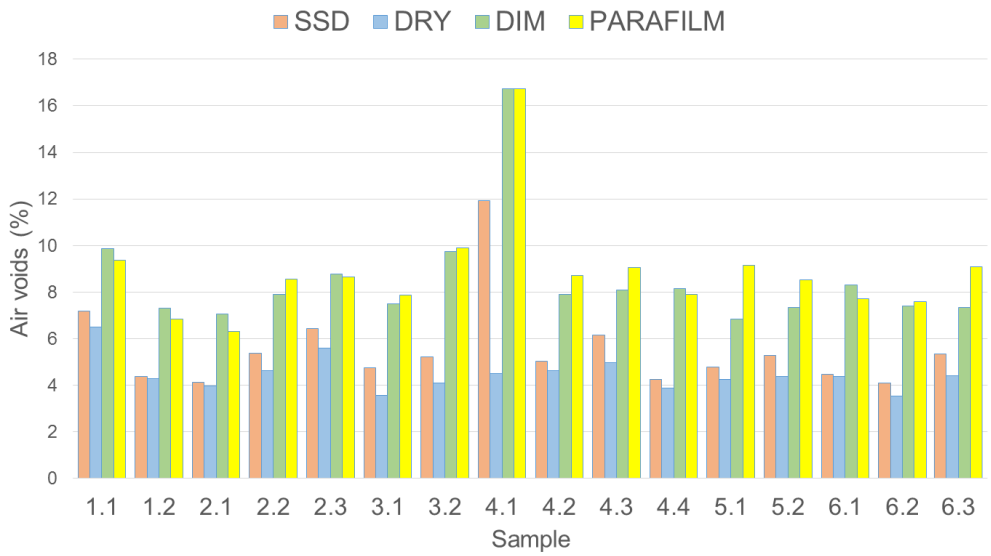

Figure 7: Comparison of different air void results of Kuopio samples

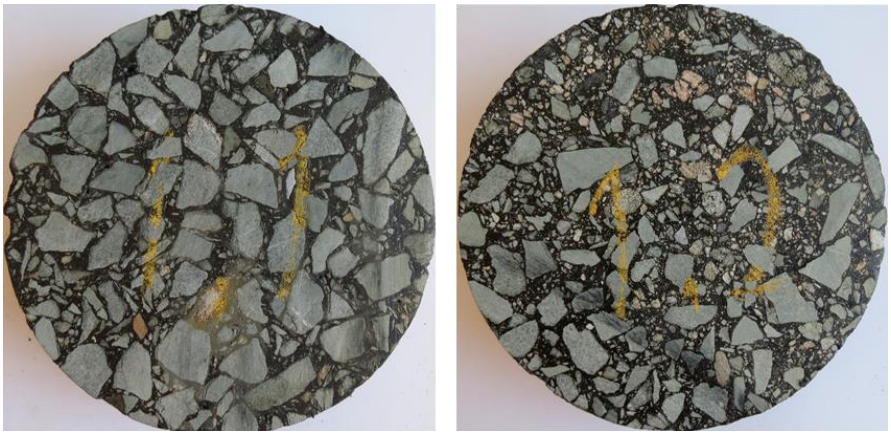

Figure 8: Top surfaces of drill core samples 1.1 and 1.2.

3.2.2 *VNA scanning results*

Four samples from Kuopio were scanned with a VNA measurement set-up. The permittivity results are shown in Table 4 and in Figure 9. Samples 3.1 and 4.3 have very high standard deviations as they are around 1.4, the averages being 6.2-6.5. This is also observed in Figure 9 as there are scanning points with high permittivities close to 9.

Table 4: Statistics of VNA measurements from selected Kuopio samples

SAMPLE	n (accepted)	n (total)	n (rejected)	mean(ε_r)	std(ε_r)
3.1	100	100	0	6.22	1.35
3.2	98	100	2	5.67	0.60
4.3	100	100	0	6.55	1.43
4.4	100	100	0	5.83	0.42
Total				6.07	1.05*

* Pooled standard deviation

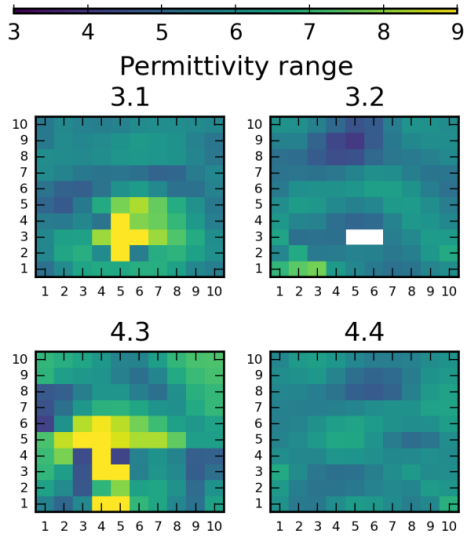

Figure 9: Permittivity scans of samples from Kuopio

3.2.3 *GPR results*

The GPR measurements with the 1 GHz antenna from the right wheel path from Kuopio are shown in Figure 10 and Figure 11. In Figure 10, gray lines indicate the locations of the drilled samples. The GPR data, provided by the contractor, was processed at Aalto University. The real part of permittivity was calculated based on the 1st half of the signal and was on average 6.38 and the standard deviation 0.46, which are close to the VNA scanning results. It can be seen from Figure

10 that a standard deviation of permittivity increases with measurement distance. This is a surprising result and may indicate some problems in the measurement system rather than variations in the measured material.

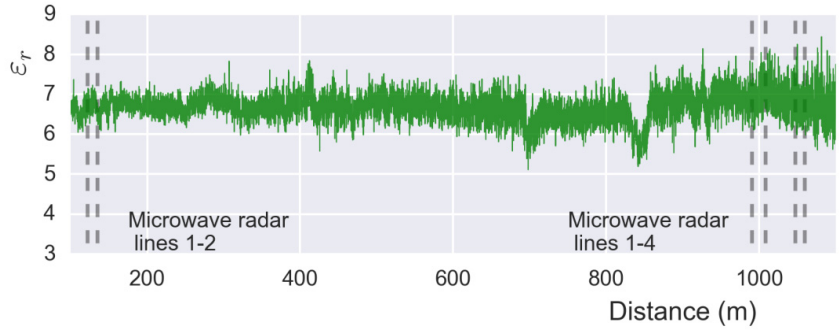

Figure 10: GPR data from Kuopio. Locations of drilled samples from 1 to 6 are marked with dashed lines from left to right

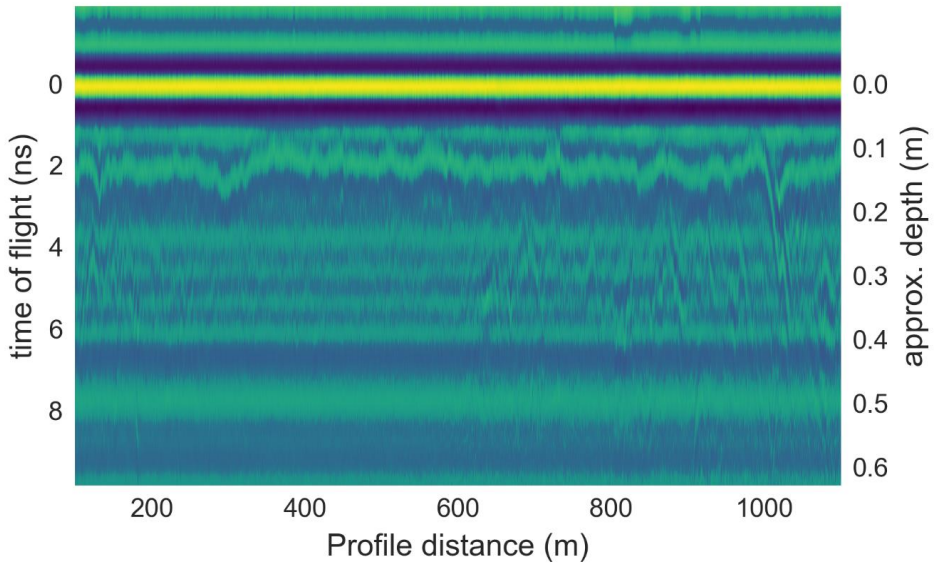

Figure 11: GPR radargram from Kuopio test site. Depth is calculated with constant permittivity 5.5

3.2.4 *Thermal camera results*

Thermal camera data from Kuopio shows variable temperatures along the pavement (Figure 12). Although some samples are taken from cold spots, their air voids do not vary clearly from other samples.

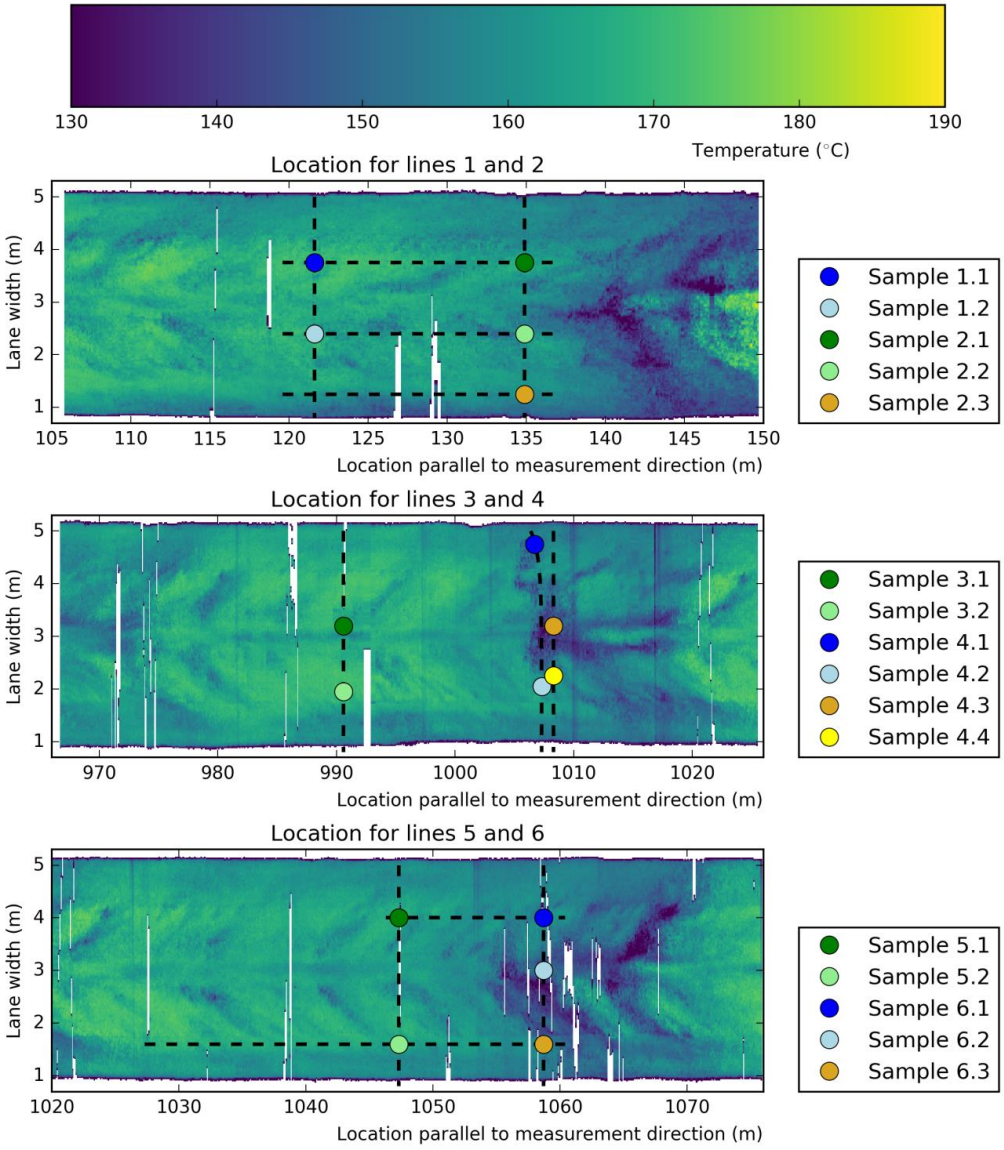

Figure 12: Thermal camera data from Kuopio. Drilled samples are marked (Failed microwave radar lines are marked with black dashed lines.)

3.2.5 *Conclusions*

Due to technical difficulties with the microwave measurements, the goal of comparing microwave radar and thermal camera results was not achieved. Otherwise, the permittivities with VNA and GPR methods showed rather high values. Usually, this might be related to the low air voids, but in this case air void contents were actually rather high. The assumed reason for higher permittivities is the rock type of the aggregates, which has a high solid density and relative permittivity. By visual inspection, the rock type was specified to be mafic to ultramafic type volcanic rock.

3.3 Yläne test site

Microwave radar testing in Yläne was part of the GPR comparison tests organized by the Finnish Transport Agency. The aim of the comparison tests was to measure the same road sections with different GPR systems, and then compare the calculated air void contents. It was not possible to measure the whole road section with the microwave radar; therefore, each drill core location was only measured 200 m at the most over from the right wheel path. The test site was located in road 210 part 9 from 4200 to 6500 meters.

Radar testing locations are shown in Figure 13. Figure 14 shows the drilling location of samples S1U_4420 and S2U_4420. Measurements were conducted for the first time on 28.7.2014. As rainfall interrupted the first measurements, measurements were conducted for the second time on 5.8.2014.

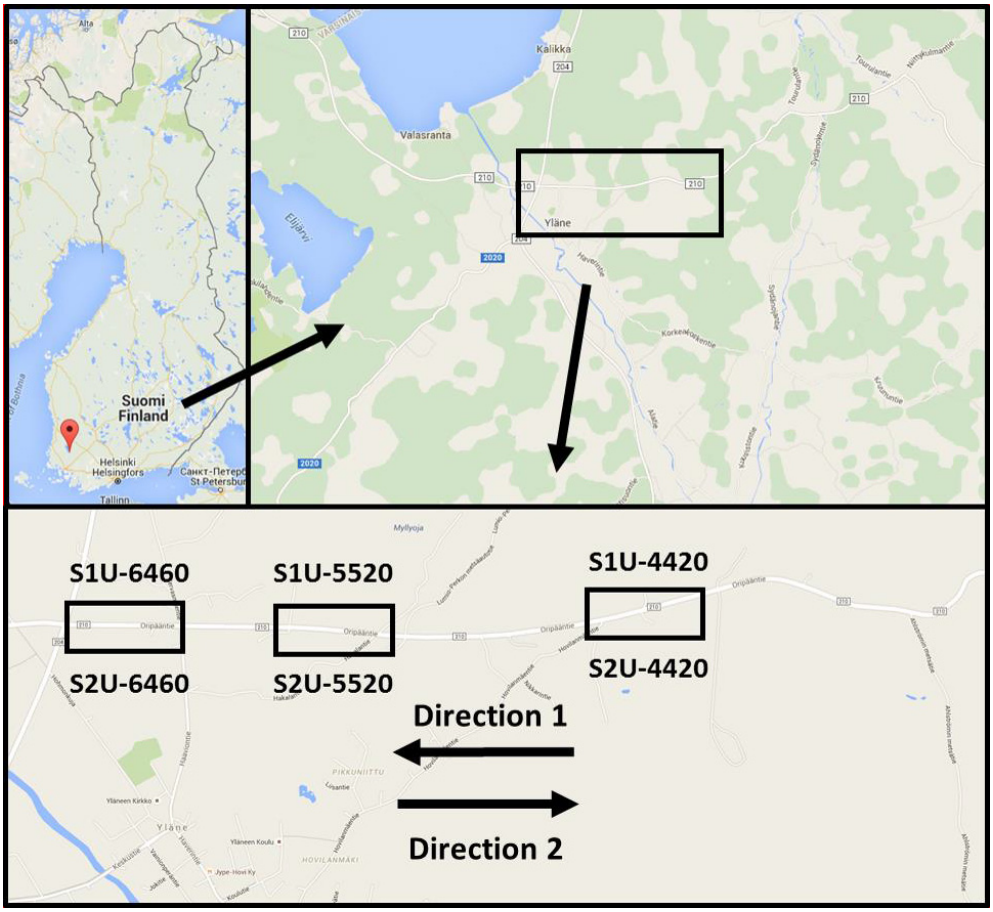

Figure 13: Locations of microwave radar measurements in Yläne test site. The aim was to measure 100 m before and after each asphalt core location from the right wheel path (Map data ©2015 Google)

Figure 14: Asphalt samples were drilled from the right wheel path and between the wheel paths. The picture shows samples S2U_4420 and S2K_4420 in the front, and samples S1U_4420 and S1K_4420 on the other lane. Two samples were taken next to each other and named a and b

3.3.1 *Density and air void results*

The bulk and maximum densities were measured in the laboratory according to (SFS-EN12697-8). Air voids were calculated based on the laboratory results. The results are presented in Table 5 and Table 6. Samples a and b were drilled side by side. The letter k in the sample name refers to the core location in the center of the wheel paths. In Figure 15, air voids determined with different methods are compared for each sample from the right wheel path. In this case, air void results are low from 0.5 to 3.5 with the dry method as the pavement was AB type. The drill core diameter was 100 mm.

Table 5: Density and air void results of drill core samples from Yläne

	G_{mb}				G_{mm}	V_a (%)			
SAMPLE	**SSD**	**DRY**	**DIM**	**PARAF.**		**SSD**	**DRY**	**DIM**	**PARAF.**
S1U_6460_a	2.454	2.452	2.424	2.412	2.482	1.1	1.2	2.3	2.8
S1U_6460_b	2.434	2.430	2.396	2.394	2.461	1.1	1.2	2.6	2.7
S2U_6460_a	2.478	2.475	2.446	2.440	2.511	1.3	1.4	2.6	2.8
S2U_6460_b	2.467	2.464	2.431	2.412	2.495	1.1	1.2	2.6	3.3
S1U_5520_a	2.449	2.444	2.409	2.401	2.498	2.0	2.2	3.5	3.9
S1U_5520_b	2.458	2.454	2.431	2.402	2.504	1.9	2.0	2.9	4.1
S2U_5520_a	2.464	2.456	2.420	2.409	2.503	1.5	1.9	3.3	3.8
S2U_5520_b	2.465	2.462	2.433	2.421	2.512	1.9	2.0	3.1	3.6
S1U_4420_a	2.421	2.424	2.389	2.357	2.493	2.9	2.7	4.2	5.4
S1U_4420_b	2.426	2.423	2.380	2.363	2.501	3.0	3.1	4.8	5.5
S2U_4420_a	2.437	2.437	2.427	2.375	2.488	2.0	2.0	2.4	4.5
S2U_4420_b	2.444	2.442	2.382	2.378	2.473	1.2	1.3	3.7	3.8
mean U_{total}	2.450	2.447	2.414	2.397	2.493	1.8	1.9	3.2	3.9
std U_{total}	0.018	0.016	0.022	0.025	0.015	0.7	0.6	0.8	0.9
S1K_6460_a	2.478	2.474	2.453	2.427	2.489	0.4	0.6	1.5	2.5
S1K_6460_b	2.485	2.482	2.464	2.453	2.495	0.4	0.5	1.2	1.7
S2K_6460_a	2.474	2.470	2.458	2.437	2.508	1.4	1.5	2.0	2.8
S2K_6460_b	2.465	2.461	2.421	2.413	2.506	1.6	1.8	3.4	3.7
S1K_5520_a	2.469	2.465	2.447	2.433	2.499	1.2	1.4	2.1	2.7
S1K_5520_b	2.477	2.473	2.449	2.435	2.501	1.0	1.1	2.1	2.7
S2K_5520_a	2.481	2.474	2.443	2.426	2.498	0.7	1.0	2.2	2.9
S2K_5520_b	2.490	2.485	2.471	2.455	2.505	0.6	0.8	1.4	2.0
S1K_4420_a	2.443	2.439	2.413	2.390	2.525	3.3	3.4	4.4	5.4
S1K_4420_b	2.441	2.438	2.397	2.382	2.526	3.4	3.5	5.1	5.7
S2K_4420_a	2.476	2.470	2.463	2.394	2.498	0.9	1.1	1.4	4.2
S2K_4420_b	2.470	2.467	2.428	2.413	2.500	1.2	1.3	2.9	3.5
mean K_{total}	2.471	2.466	2.442	2.421	2.504	1.3	1.5	2.5	3.3
std K_{total}	0.015	0.015	0.023	0.024	0.011	1.0	1.0	1.2	1.3
mean $_{total}$	2.460	2.457	2.428	2.409	2.499	1.5	1.7	2.8	3.6

std $_{total}$	0.019	0.018	0.026	0.027	0.014	0.9	0.8	1.1	1.1

Table 6: Solid density results of drill core samples from Yläne

	SOLID DENSITY		
SAMPLE	**< 0.125 mm**	**4-11.2 mm**	**11.2 mm >**
S1U_6460_b	2.690	2.690	2.716
S2U_5520_b	2.698	2.689	2.723

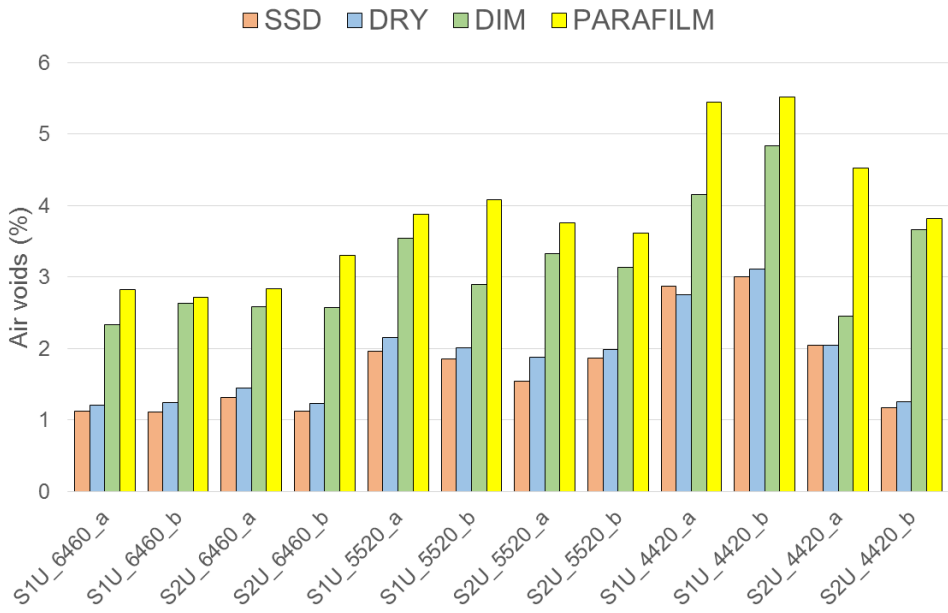

Figure 15: Comparison of different air void results of samples from Yläne

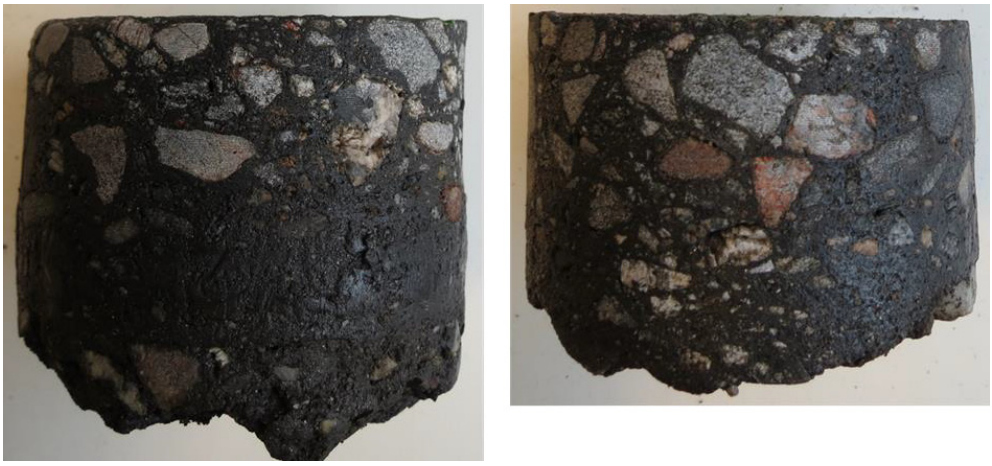

Figure 16: Drillcore samples S1U_6460_b and S2U_5520_b

3.3.2 *VNA scanning results*

The b-samples from the right wheel path were scanned with the VNA measurement set-up. The permittivity results are shown in Table 7 and in Figure 17. Some of the measurement points from the upper right corner were excluded from the results, because the scanning area was too close to the sample edge, therefore distorting the results. The average permittivity of the VNA scanning vary between 5.11 and 6.05. With these samples, no very high permittivities were obtained, which is seen as lower standard deviation values.

Table 7: Statistics of VNA measurements of selected samples from Yläne

SAMPLE	n (accepted)	n (total)	n (rejected)	mean(ε_r)	std(ε_r)
S1U_6460_b	100	100	0	5.11	0.35
S2U_6460_b	97	100	3	5.78	0.58
S1U_5520_b	97	100	3	5.38	0.80
S2U_5520_b	92	100	8	5.15	0.54
S1U_4420_b	95	100	5	6.05	0.55
S2U_4420_b	98	100	2	5.60	0.78
Total				5.51	0.62*

* Pooled standard deviation

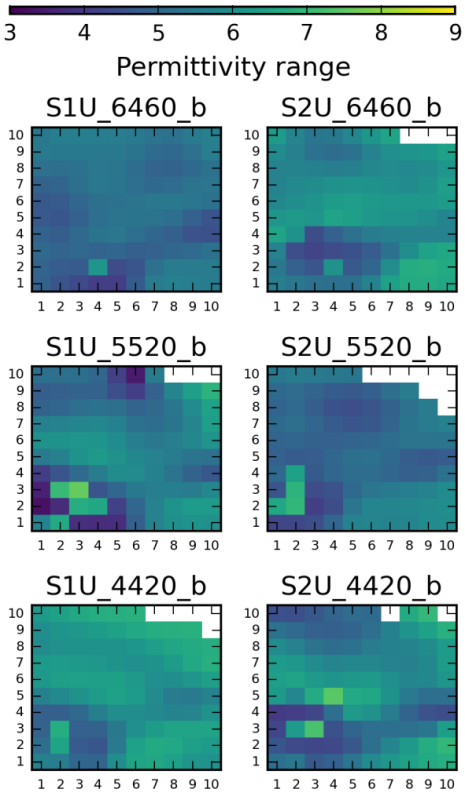

Figure 17: Permittivity scans of samples from Yläne

3.3.3 *Microwave radar results*

Altogether, six locations in Yläne were measured with the microwave radar. Since rainfall interrupted the measurements on 28.7.2014, two locations were measured on 5.8.2014 and another two locations were re-measured. The radar results are presented as violin plots in Figure 18 and kernel density estimations in Figure 19. The black line inside the violin plot indicates the median value of the distribution. The median of different measurements ranged between 3 and almost 5. The distribution of permittivity values seems to vary from one measurement location to another. The general estimated kernel density shapes from lines S1U_6460 and S2U_6460, which were measured two times, are in agreement with each other. A slight increase of permittivity is evident for the second measurement time, which could be a result of different moisture content in the pavement structure.

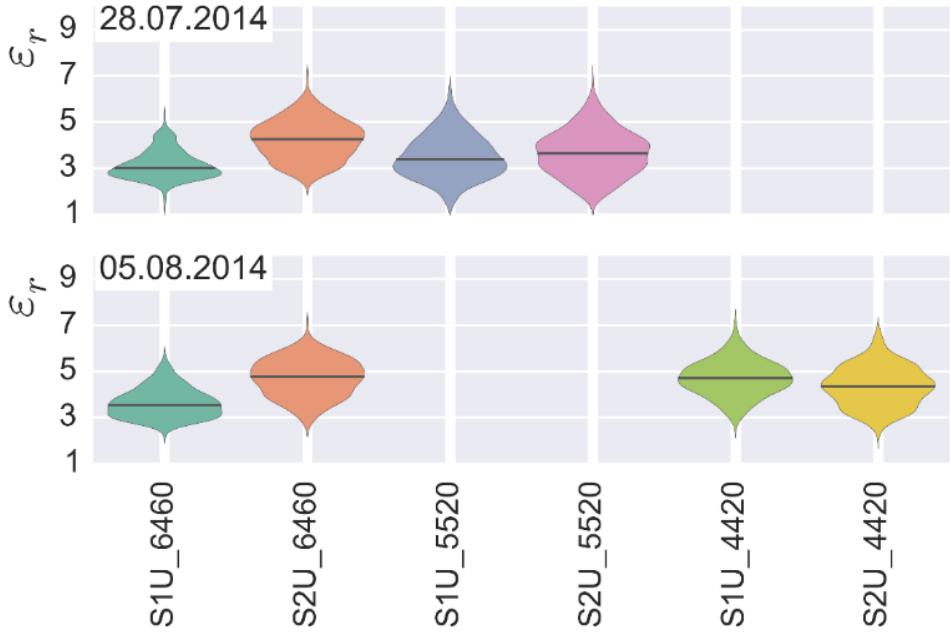

Figure 18: Microwave results from Yläne

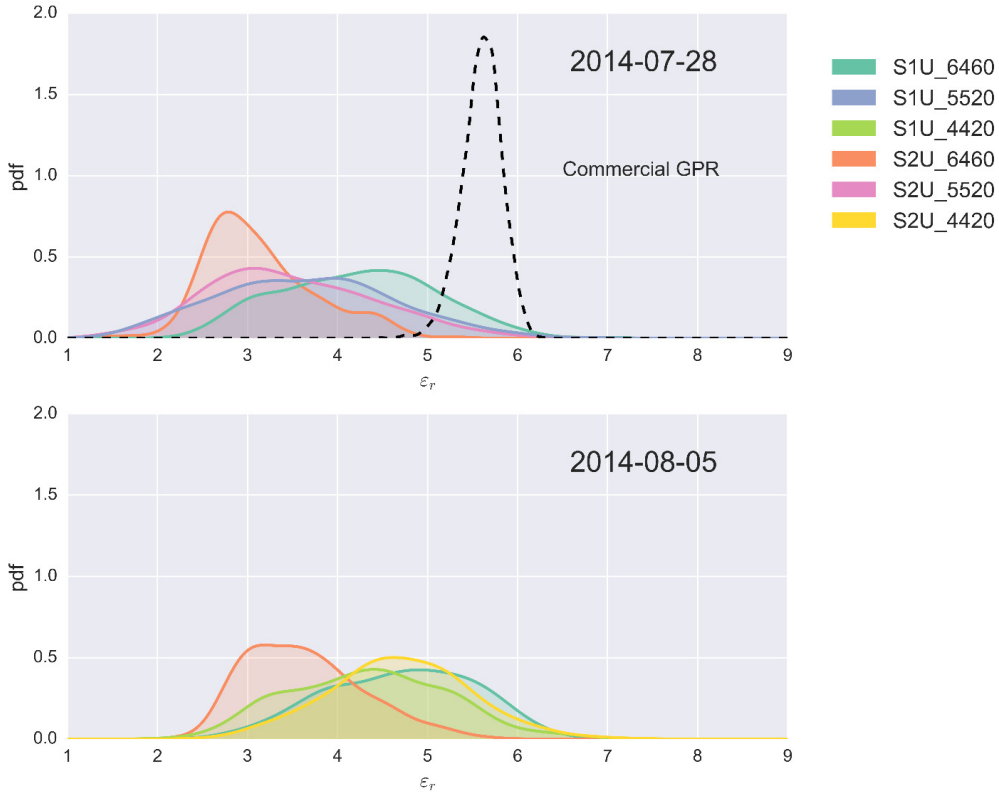

Figure 19: Kernel density estimations of microwave radar measurements

3.3.4 *GPR results*

The GPR results for the right wheel path near the drill core samples are shown in Figure 20 and for S1U_1 the radargram is shown in Figure 21. The drill core sample places are marked with a dashed vertical line. The GPR data was provided by the contractor and then processed by Aalto University. The average permittivity value measured with the GPR was 5.59 with standard deviation of 0.25.

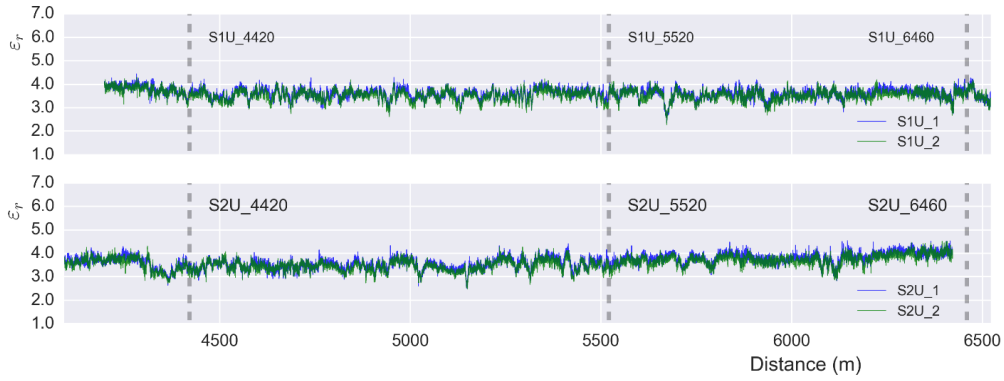

Figure 20: GPR data from RWP Yläne. Locations of drilled samples are marked with dashed lines

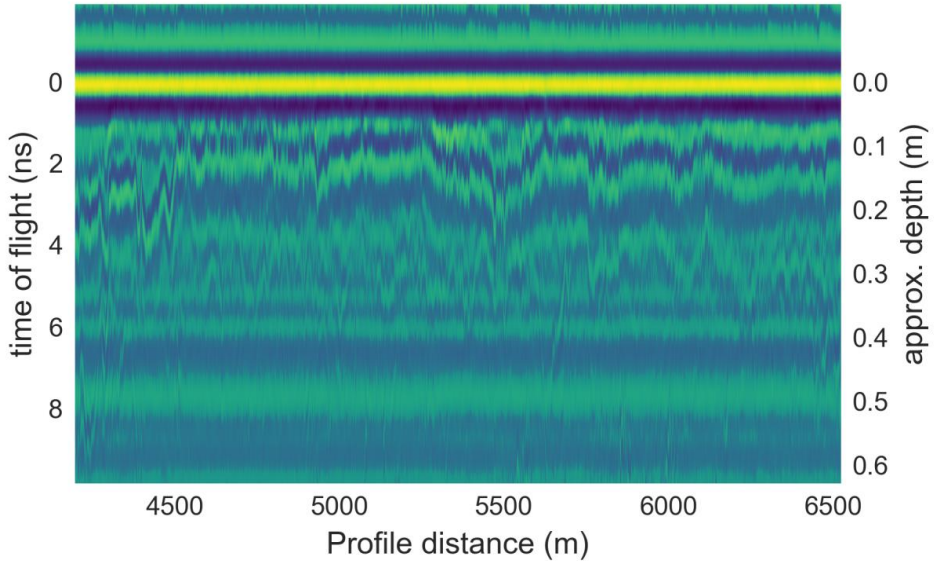

Figure 21: GPR radargram from Yläne S1U_1. Depth is calculated with constant permittivity 5.5.

3.3.5 *Conclusions*

The air void content of asphalt samples was rather low for all samples. The permittivity results from the VNA measurement are on average closer to the GPR measurements than the microwave results. The microwave radar results seem to be on a different level as their median permittivities are clearly less than 5. This level change might be the result of a different measurement fingerprint than that of the microwave radar and GPR. The microwave radar is more sensitive to the roughness

of the road as well as to the pavement surface material content and its grain size. The VNA measures through a sample which means that the permittivity result presents the whole sample.

3.4 Hamina test site

To be able to verify the sufficient depth resolution with the microwave radar, radar testing was performed in a road construction site, where it was possible to measure each pavement layer separately after each phase of construction. The chosen road section in Hamina is on a four-lane motorway (Figure 22 a). The constructed road layers (Figure 22 b) are:

- crushed base (measured 30.7.2014; microwaver radar)
- $AC_{base}1$ layer on driving lane and crushed base on the passing lane (measured 1.8.2014; microwaver radar)
- $AC_{base}2$ layer (measured 22.8.2014; microwaver radar)
- second AC layer (measured 3.9.2014; microwaver radar)
- SMA wearing course (measured 16.6.2015; microwaver radar, GPR).

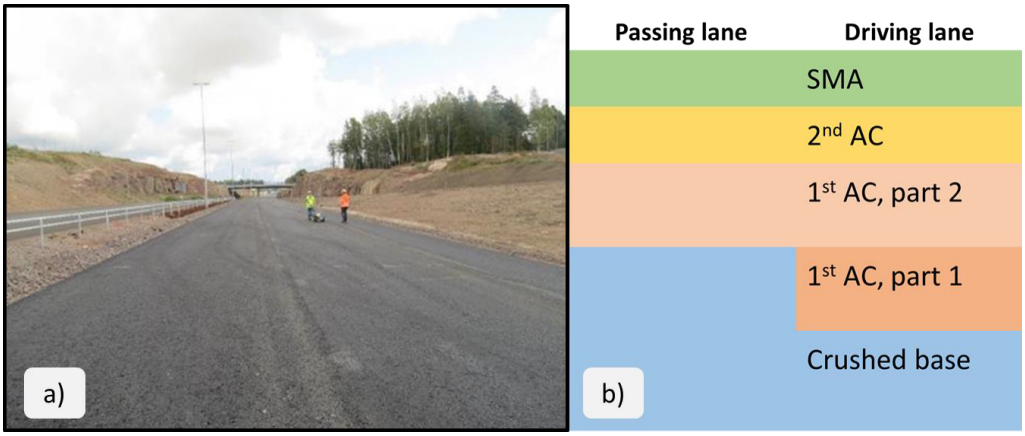

Figure 22: a) The picture was taken 22.8.2014 when $AC_{base}2$ layer was measured with the microwave radar, b) Schematic figure of the road structure

Figure 23: Map from Hamina test site (Map data ©2016 Google)

The test site was located on Road 5 part 34 approximately 100 to 200 meters. The same 104 m long highway section was measured on each measurement time. Measurements were undertaken with the 12-18 GHz radar. There were 5 parallel measurement lines. As shown in Figure 24, lines 1, 2 and 3 were measured from the driving lane (Lane 1), and they correspond approximately to the RWP, CWP and LWP. Lines 4 and 5 were measured from the passing lane (Lane 2) and they correspond approximately to the LWP and the RWP.

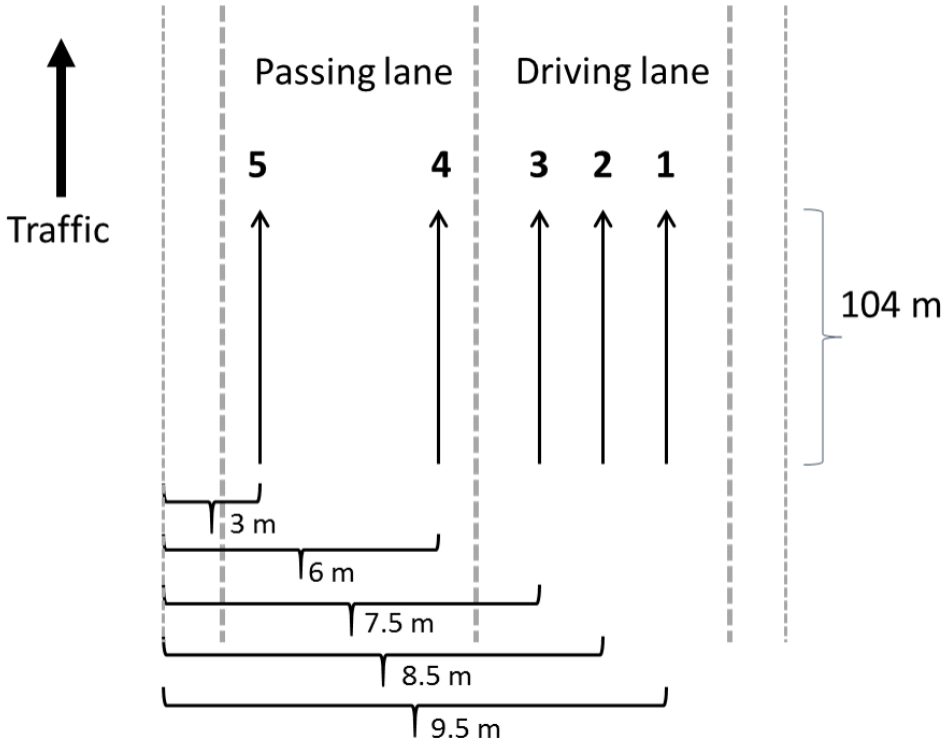

Figure 24: Radar measurement lines are numbered from 1 to 5. Each line was 104 m long

The contractor took drilled core samples in the autumn of 2014 after all the AC layers were constructed. The sampling was limited to two 150 mm drill core samples (L-1, L-2) through all asphalt pavement layers. In addition, eight 100 mm samples (S-1 to S-8) were drilled. The samples S-1—S-2 and S-5—S-6 are thinner since the road structure is different on Lane 2. The sampling is presented in Figure 25 a, and the naming of the drill core in Figure 25 b.

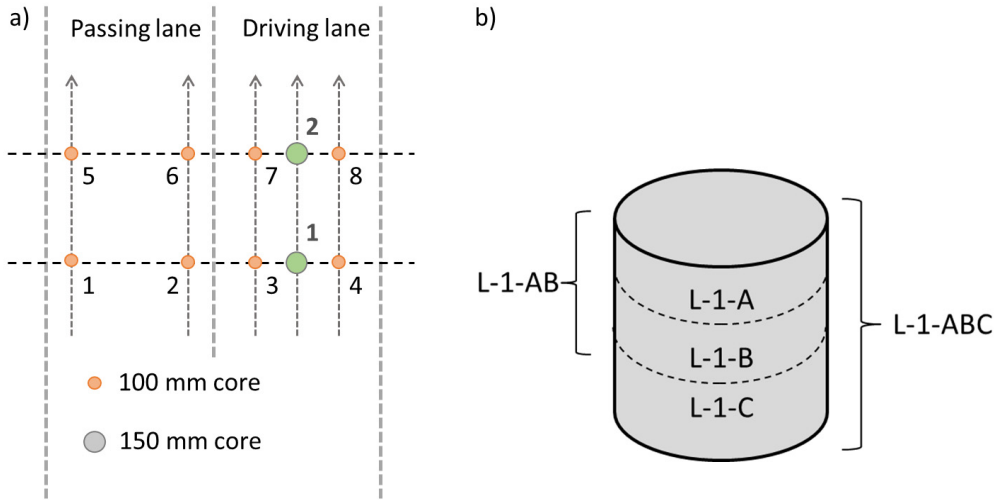

Figure 25: a) Map of the sampling in Hamina, b) Schematic figure indicating the method of naming drilled samples for laboratory measurements

3.4.1 *Density and air void results*

The bulk and maximum densities were measured in the laboratory according to (SFS-EN 12697-8). Air voids were calculated based on the laboratory results. The laboratory measurements show that on the driving lane the AC_{base}1-layer has on average the highest bulk density, 2.396 Mg/m^3. The 2nd AC-layer has the lowest bulk density on average, 2.307 Mg/m^3, and the AC_{base}2-layer has the average bulk density between the AC_{base}1 and 2nd AC-layer, 2.335 Mg/m^3. On the passing lane, the highest average bulk density is with the 2nd AC-layer, on average 2.380 Mg/m^3, and the AC_{base}2-layer has a density on average 2.345 Mg/m^3. All the results are presented in Table 8 and Table 9.

Table 8: Density and air void results of drill core samples from Hamina

	G_{mb}			G_{mm}	V_a %		
SAMPLE	**SSD**	**DRY**	**DIM**		**SSD**	**DRY**	**DIM**
L-1-ABC	2.325	2.351	2.279	2.461	5.5	4.5	7.4
L-1-AB	2.300	2.322	2.266	2.446	6.0	5.1	7.4
L-1-A	2.275	2.287	2.219	2.418	5.9	5.4	8.2
L-1-B	2.335	2.357	2.308	2.472	5.5	4.7	6.6
L-1-C	2.376	2.383	2.321	2.484	4.3	4.1	6.6
L-2-ABC	2.325	2.356	2.292	2.462	5.6	4.3	6.9
L-2-AB	2.286	2.318	-	2.449	6.6	5.3	-
L-2-A	2.253	2.276	2.202	2.421	6.9	6.0	9.0
L-2-B	2.338	2.349	2.318	2.473	5.5	5.0	6.2

L-2-C	2.404	2.404	-	2.484	3.2	3.2	-
S-1-A	2.382	2.381	2.337	2.421	1.6	1.7	3.5
S-1-B	2.322	2.336	2.199	2.464	5.8	5.2	10.8
S-2-A	2.383	2.379	2.371	2.415	1.3	1.5	1.8
S-2-B	2.393	2.395	2.323	2.475	3.3	3.2	6.1
S-3-A	2.398	2.395	2.369	2.427	1.2	1.3	2.4
S-3-B	2.312	2.364	2.282	2.489	7.1	5.0	8.3
S-3-C	2.374	2.375	2.247	2.474	4.0	4.0	9.2
S-4-A	2.320	2.346	2.303	2.462	5.8	4.7	6.5
S-4-B	2.282	2.307	2.227	2.431	6.1	5.1	8.4
S-4-C	2.418	2.417	2.392	2.463	1.8	1.9	2.9
S-5-A	2.376	2.373	2.350	2.423	1.9	2.1	3.0
S-5-B	2.283	2.337	2.181	2.478	7.9	5.7	12.0
S-6-A	2.379	2.378	2.348	2.439	2.5	2.5	3.7
S-6-B	2.386	2.397	2.304	2.478	3.7	3.3	7.0
S-7-A	2.342	2.341	2.306	2.427	3.5	3.5	5.0
S-7-B	2.344	2.356	2.331	2.473	5.2	4.7	5.7
S-7-C	2.390	2.396	2.226	2.486	3.9	3.6	10.5
S-8-A	2.359	2.363	2.347	2.467	4.4	4.2	4.9
S-8-B	2.300	2.307	2.271	2.427	5.2	4.9	6.4
S-8-C	2.413	2.413	2.376	2.470	2.3	2.3	3.8
A_{mean}	2.346	2.351	2.275	2.467	5.6	4.7	7.7
A_{std}	0.049	0.029	0.052	0.020	1.3	0.8	1.8
B_{mean}	2.329	2.350	2.273	2.466	5.5	4.7	7.8
B_{std}	0.038	0.031	0.054	0.020	1.4	0.8	2.1
C_{mean}	2.396	2.398	2.310	2.477	3.3	3.2	6.6
C_{std}	0.019	0.017	0.074	0.009	1.0	0.9	3.3
$Total_{mean}$	2.354	2.365	2.300	2.457	4.2	3.7	6.3
$Total_{std}$	0.045	0.035	0.060	0.025	1.9	1.4	2.8

Table 9: Solid density results of drill core samples from Hamina

	SOLID DENSITY		
SAMPLE	**< 0.125 mm**	**4-11.2 mm**	**11.2 mm >**
L-2-A	2.607	2.633	2.654
L-2-B	2.676	2.626	2.643
L-2-C	2.681	2.628	2.639

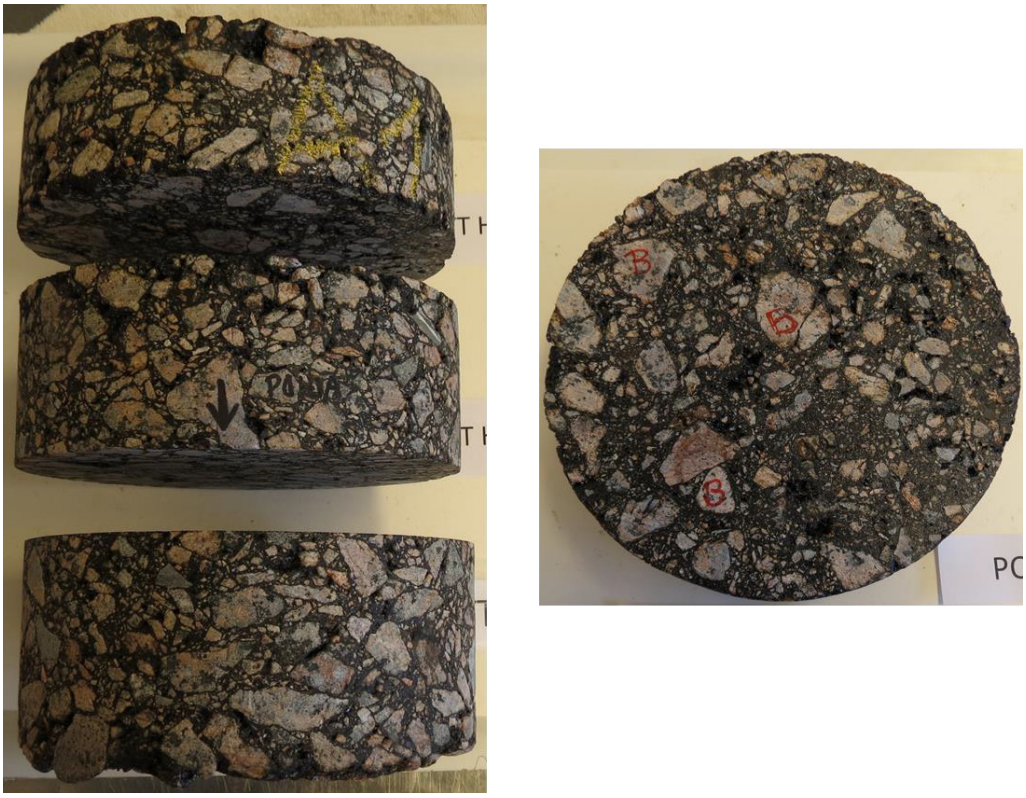

Figure 26: Drill core samples L-1-ABC and bottom of the L-1-A sample

3.4.2 *VNA scanning results*

The samples L-1 and L-2 were scanned with the VNA measurement set-up. The entire sample was separately scanned as well as each sliced layer. The measurements with VNA reveal that the $AC_{base}1$-layer has the highest average permittivity of 5.53, and the average standard deviation 0.74. The permittivity of the $AC_{base}2$-layer has an average permittivity value of 5.27 which is lower than for the first layer. The standard deviation on average is 0.74 which is equal compared to the $AC_{base}1$-layer. The 2nd AC-layer has the lowest average permittivity with the value of 5.23, and with the standard deviation of 0.86. The results are shown in Table 10 and in Figure 27.

Table 10: Statistics of VNA measurements

SAMPLE	n (accepted)	n (total)	n (rejected)	mean(ε_r)	std(ε_r)
L-1-ABC	100	100	0	5.41	0.53
L-1-AB	100	100	0	5.68	0.70
L-1-A	100	100	0	4.94	0.82
L-1-B	100	100	0	5.40	0.80
L-1-C	100	100	0	5.34	0.46
L-2-ABC	100	100	0	5.23	0.45
L-2-AB	100	100	0	4.88	0.41
L-2-A	100	100	0	5.52	0.89
L-2-B	100	100	0	5.14	0.68
L-2-C	100	100	0	5.72	0.94
Total				5.34	0.78*

* Pooled standard deviation

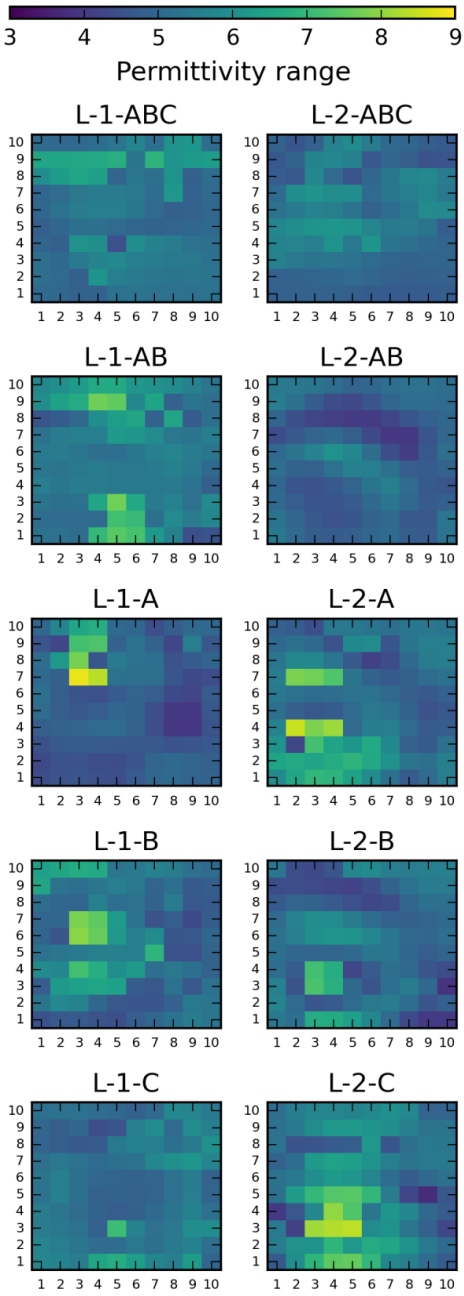

Figure 27: Permittivity scans of samples L-1 and L-2 from Hamina

3.4.3 *Microwave radar results*

The road section in Hamina was measured after each lift of construction with the microwave radar. Lines 4 and 5 could not be measured on 16.6.2015 because the lane was open to traffic. The general trend based on the microwave radar measurements shows that the AC_{base}1-layer has the lowest permittivity values with an average permittivity of 3.4, and the average of the permittivity values increased to 4.5-4.8 for the rest of the AC-layers. The radar results are presented as violin plots in Figure 28 and kernel density estimations in Figure 29. The black line inside the violin plot shows the median.

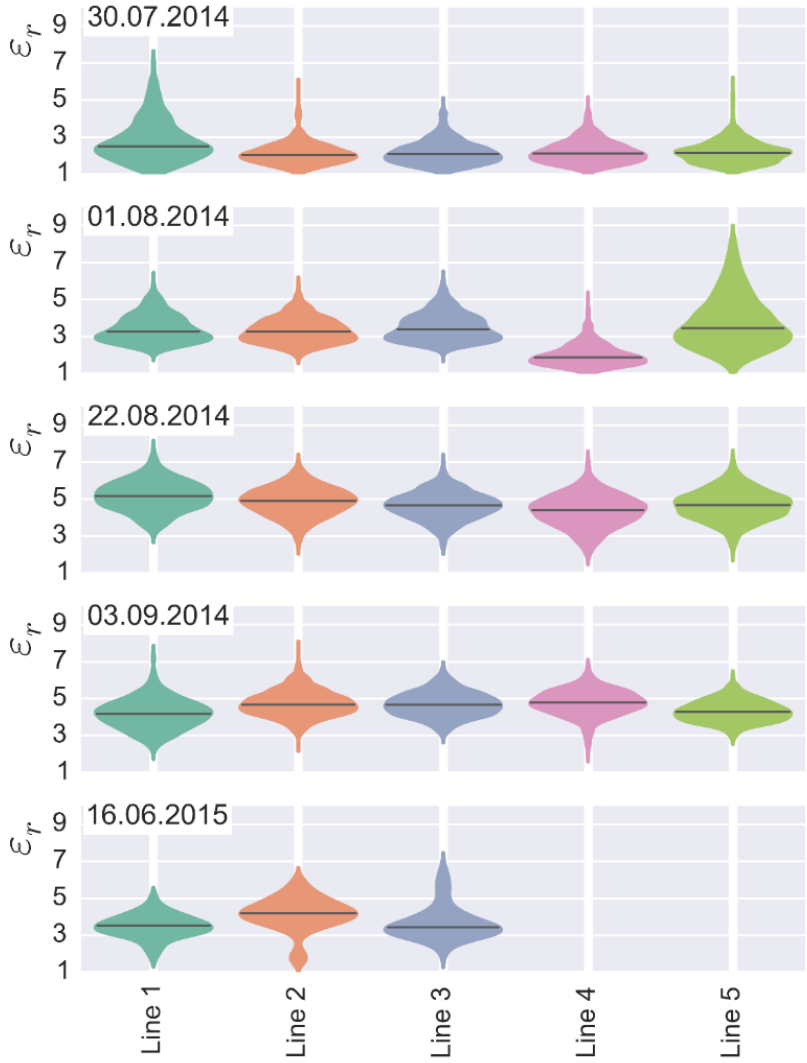

Figure 28: Microwave results from Hamina after each lift of construction

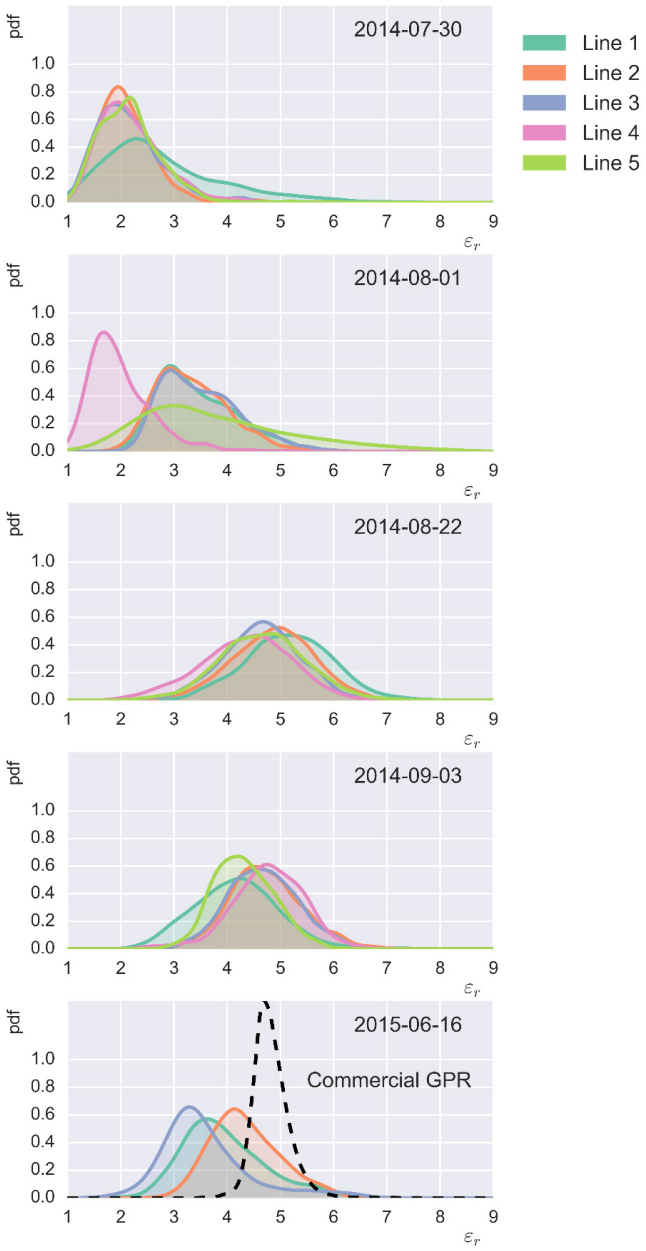

Figure 29: Kernel density estimations of microwave radar results from Hamina after each lift of construction

The mean value and standard deviation of the measurements done on line 1 are shown in Figure 30. There the results indicate that the microwave and GPR provide similar results based on the average and standard deviation.

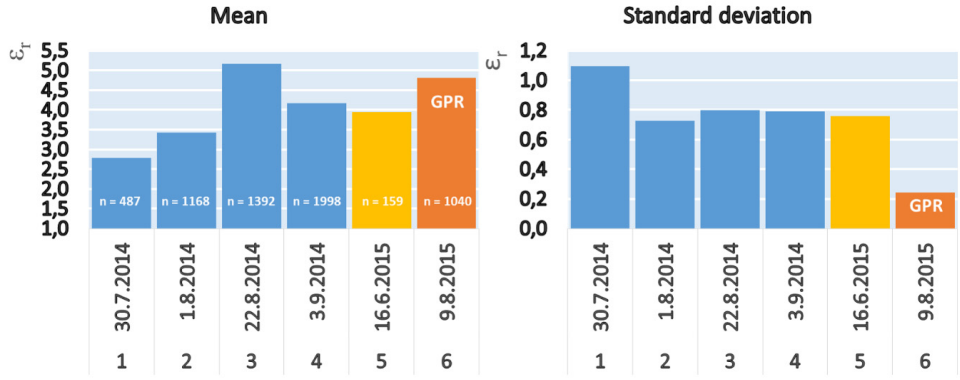

Figure 30: Mean and standard deviation of the microwave and GPR measurement on lane 1 with different times. The blue columns have been measured on AC-layers and the yellow and orange columns are measured on the same SMA-layer. The orange columns present the GPR results

3.4.4 *GPR results*

The GPR measurements in Hamina were done on Lane 1 and Lane 2 over the SMA-pavement layer. The permittivities were calculated by the Aalto University and are shown in Figure 31 and the radargram for Lane 1 is shown in Figure 21. The commercial GPR system with the permittivity calculated from the first half of the signal has the average permittivity of 4.82 when the microwave radar measurements have the average permittivity of 3.94. The standard deviations are 0.24 and 0.76, for GPR and microwave radars, respectively. Based on the second half of the GPR signal, the average permittivity is 5.51 with the standard deviation of 0.45. The average and the standard deviation are higher compared to the result from the first half of the signal. The comparison between microwave radar and GPR is shown in Figure 30.

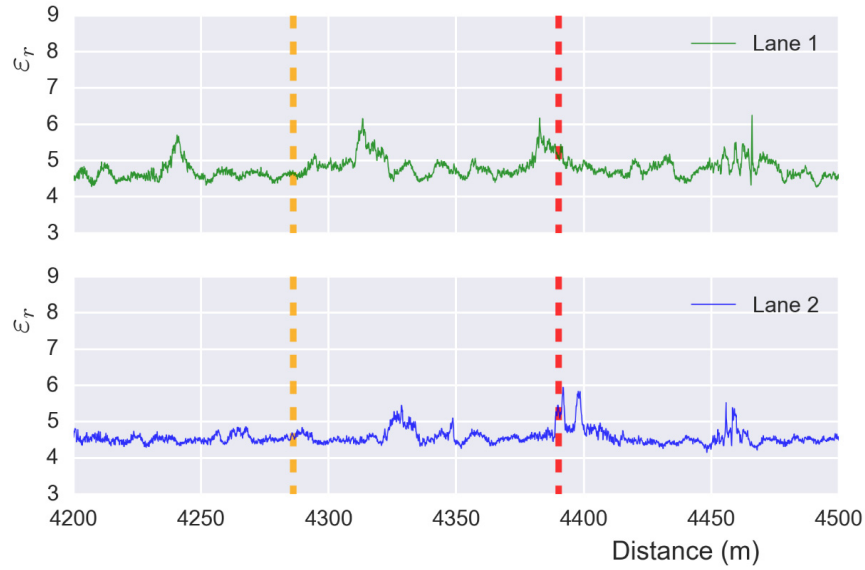

Figure 31: GPR RWP data from Hamina. Location of start (orange) and end (red) of the microwave measurement lines are marked with dashed lines. Permittivities have been calculated from the first half of the signal

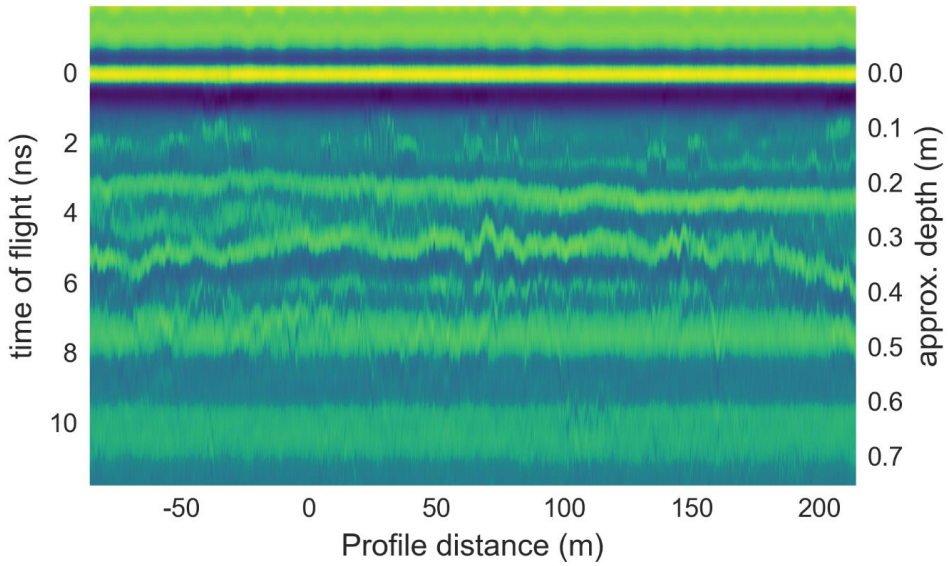

Figure 32: GPR radargram from Hamina test site. Depth is calculated with constant permittivity 5.5

3.4.5 *Conclusions*

The permittivity values measured with GPR are larger than the results measured with the microwave radar. The permittivities measured with microwave radar and VNA scanner reveal an inverted relationship. The AC_{base}1-layer has the lowest average permittivity when results from the microwave radar are used, but on average have the highest permittivities. The highest permittivities from the microwave radar measurements are with the AC_{base}2-layer when the drill core samples indicate that the average permittivities are between the highest and lowest results.

The air void contents calculated on the basis of the average maximum and bulk densities do not indicate any clear relationship with the VNA permittivity measurements. The results contain a significant amount of variability, which affects the conclusion about the exact relationship between the permittivity as well as the bulk and maximum densities.

3.5 Koskenkylä quarry reference measurements

The aim of the Koskenkylä reference measurements was to study the amplitude measurement performance of the commercial GPR system and the depth resolution. If the depth resolution is inadequate, the calculated permittivity might provide exceptionally high or low values. Reference measurements were conducted in the Koskenkylä crushing plant. The measurement setup consisted of 0.3 m thick crushed rock layer, 60 mm reference material, 10 mm metallic plate and a commercial GPR with two antennas in 1 and 2 GHz center frequencies. There were two measurement setups for each antenna. The first setup consisted of measurements of the crushed rock layer and a metal plate for the reference above the crushed rock shown in Figure 33 a and b. The second setup consisted of a reference material above the crushed rock layer and a metal plate over the reference material shown in Figure 33 c and d. The permittivities for crushed rock and the reference material were calculated based on the first and second signal half separately using the metal plate as a reference. The known permittivity of the reference material, based on laboratory measurements with VNA, is 2.85.

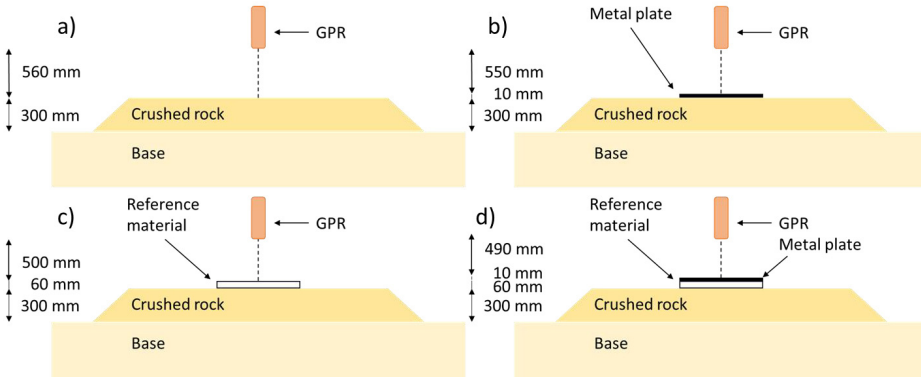

Figure 33: Koskenkylä reference measurement setup, a) crushed rock, b) crushed rock with metal plate reference, c) crushed rock with reference material and c) crushed rock and reference material with metal plate

Figure 34: Measurement setup for POM-plate, metal plate on crushed rock, and crushed rock only

3.5.1 *Reference measurements results*

The calculated permittivities for 1 GHz shown in Figure 37 describe the variation of the permittivity measurements. The first signal half has a lower calculated permittivity compared to the second signal half. On average, the first signal half correctly measures the reference material and the

second signal half overestimates the permittivity. At 2 GHz, the radar shows more variation in measurement results when compared to the 1 GHz results. For the reference material, the 2 GHz radar overestimates the permittivity with both signal halves. The 1 GHz and 2 GHz results are presented in Table 11.

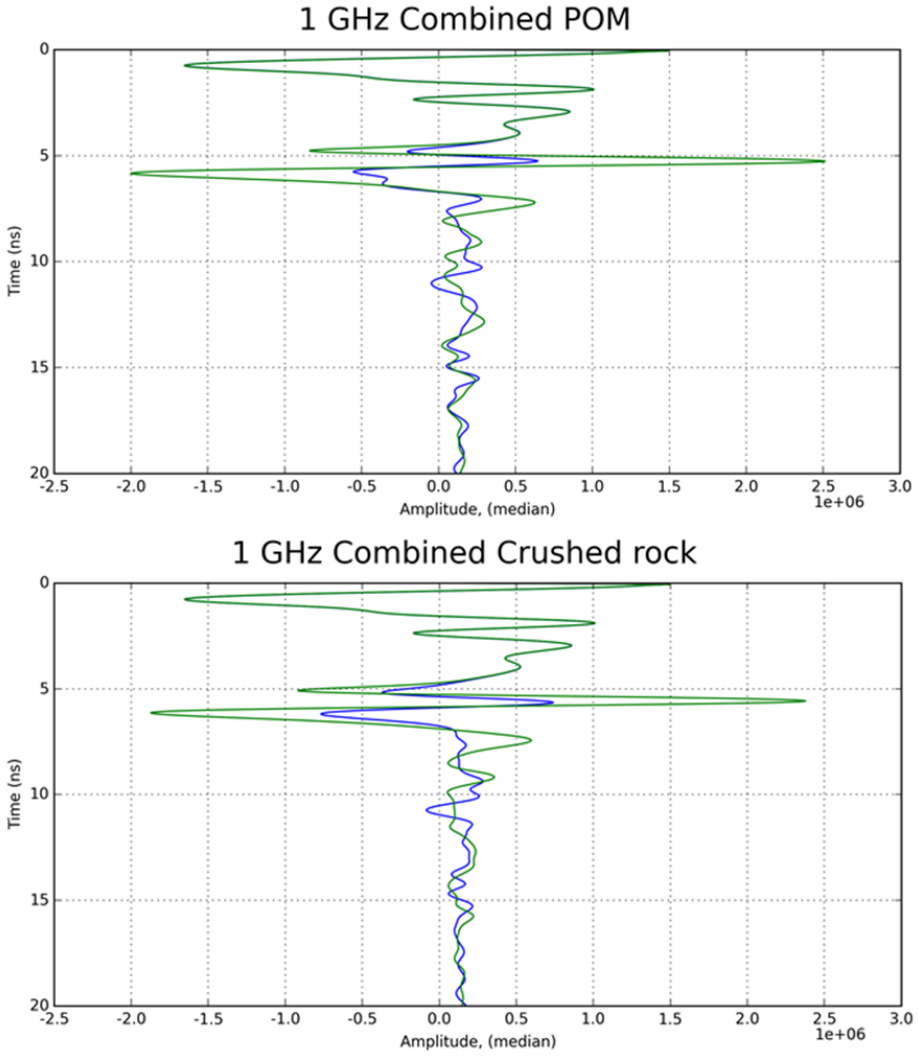

Figure 35: Median amplitude in time domain for the 1 GHz radar with POM and crushed rock. Metal peaks are shown in green and material measurement in blue. The surface reflection is seen near the 5 ns mark

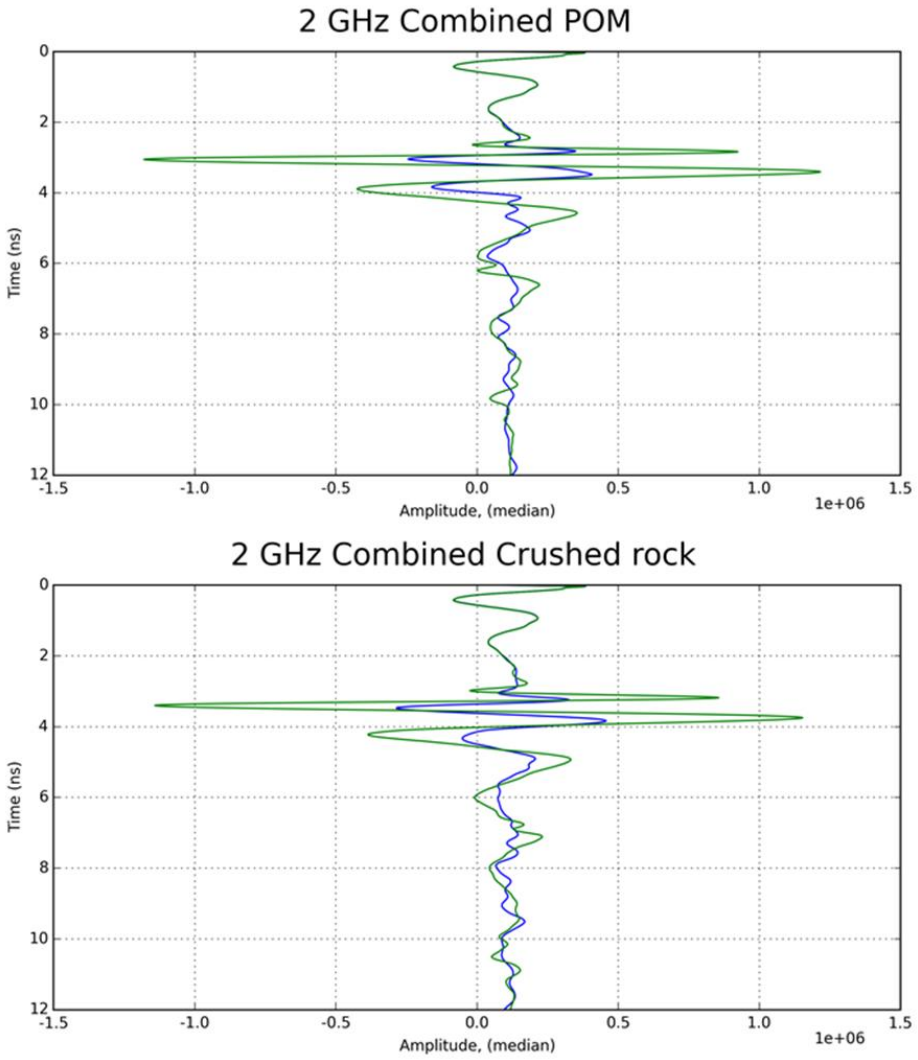

Figure 36: Median amplitude in time domain for 2 GHz with POM and crushed rock. Metal peaks are shown in green and material measurement in blue. The surface reflection is seen near 4 ns mark

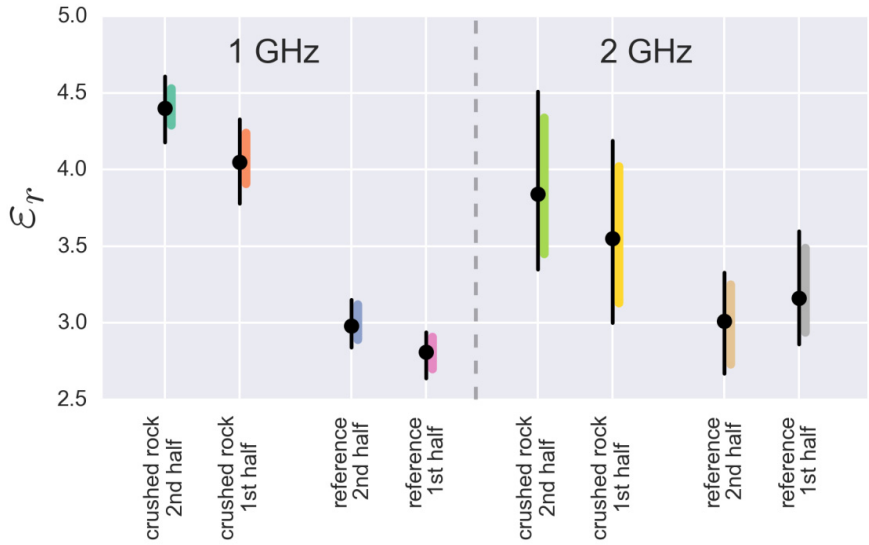

Figure 37: Koskenkylä reference measurement results for 1 and 2 GHz radar. The colored vertical lines describe variations in measured permittivity due to measurement accuracy with mean metal reflection as reference. The black vertical line shows variation when variation in metal reflection has been taken into account. Black dots show the permittivity calculated with mean values

Table 11: Koskenkylä reference measurement results

Frequency	Signal half	Material	Mean	Min	Max	Min (metal)*	Max (metal)*
1 GHz	1st	Crushed rock	4.40	4.29	4.53	4.18	4.61
1 GHz	2nd	Crushed rock	4.05	3.91	4.24	3.78	4.33
1 GHz	1st	Reference	2.98	2.89	3.12	2.84	3.15
1 GHz	2nd	Reference	2.81	2.70	2.91	2.64	2.94
2 GHz	1st	Crushed rock	3.84	3.45	4.34	3.35	4.51
2 GHz	2nd	Crushed rock	3.55	3.13	4.02	3.00	4.19
2 GHz	1st	Reference	3.01	2.73	3.25	2.67	3.33
2 GHz	2nd	Reference	3.16	2.94	3.49	2.86	3.60

* Permittivity calculated with the minimum/maximum of the metal reflection as a reference

3.5.2 *Conclusions*

According to the reference measurements, the permittivity values for the reference material are excessively high. The cause of this is the interference of two reflections: the surface reflection and the deeper reflection. This phenomenon may occur when the signal pulse width is more than two times the layer thickness. Due to this behavior, the 1 GHz results obtained from the first signal half might be coincidental. Observed erroneous permittivity values of the reference plate indicate severe problems in obtaining meaningful results of compacted asphalt layers if the depth of the pavement layer is not considered.

The amplitude measurement performance indicates that the permittivity calculated with average metal reflection varies 0.3 units with 1 GHz antenna and 0.7 units with 2 GHz antenna. With minimum and maximum reflections included in the metal reflections, the calculated permittivity variations are 0.4 and 0.9 units, 1 GHz and 2 GHz antennas, respectively.

3.6 Vt 3 and Vt 12 GPR repeat measurements

The GPR measurement at Vt 3 and Vt 12, reported earlier, were repeated in 2015. The aim of the repeat measurements was to study the temporal changes in permittivity. For Vt 3, the right and the center wheel paths (RWP, CWP) on the driving lane were measured, and for Vt 12, the right wheel path on the driving lane. The measurements were conducted with the same 1 GHz antenna by the commercial GPR apparatus as earlier, although the antenna was mistakenly mentioned as being 2.2 GHz in the previous report.

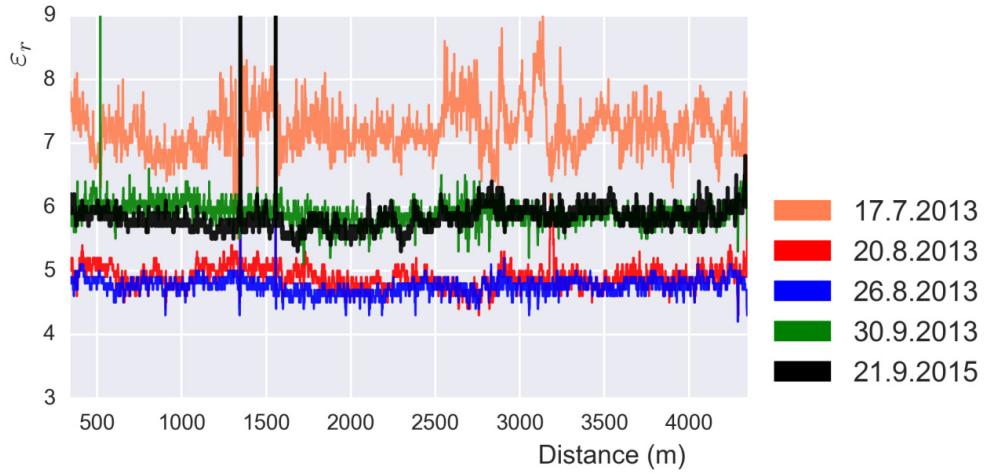

Figure 38: Vt 3 permittivity measurements in different times. The RPW 1-4 are originally presented in the previous report (Pellinen et al 2015) and the latest measurement is shown in black. Distance runs from west to east

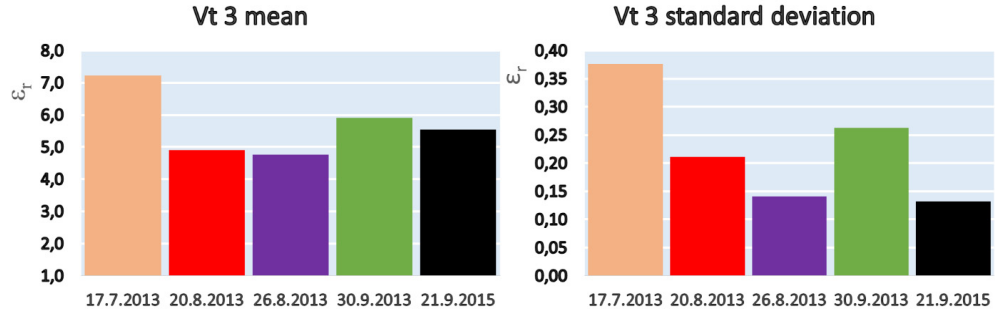

Figure 39: Vt 3 mean and standard deviation values corresponding to the measurements done in 2013 and 2015

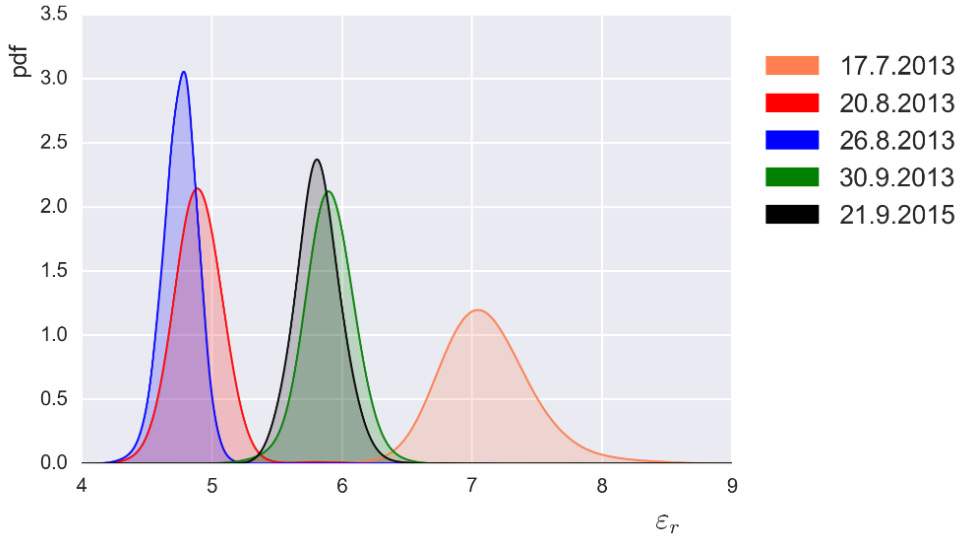

Figure 40: KDE of data GPR data from Vt 3 measured in 2013 and 2015

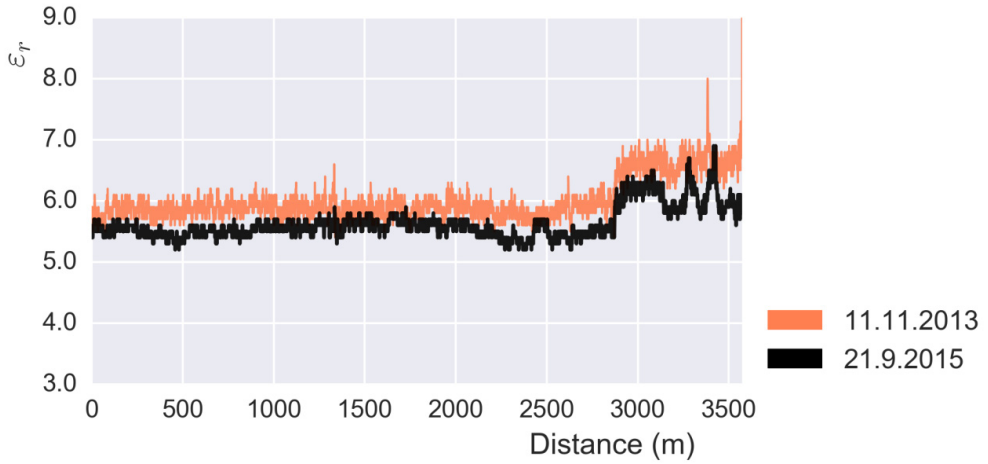

Figure 41: Vt 12 permittivity measurements from RWP in 2013 (orange) and 2015 (black). Distance is running in the direction of Tampere to Pori

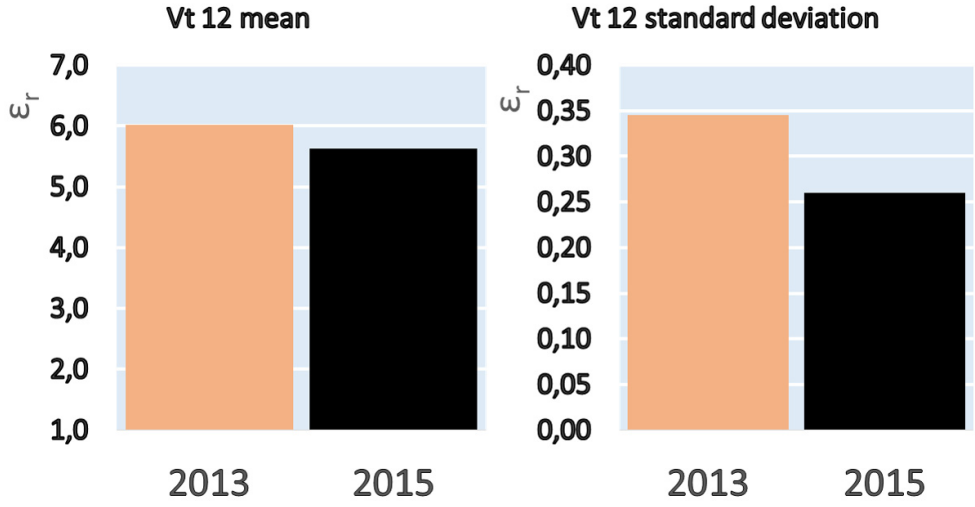

Figure 42: Vt 12 mean and standard deviations for the measurements done in 11.11.2013 and 21.9.2015

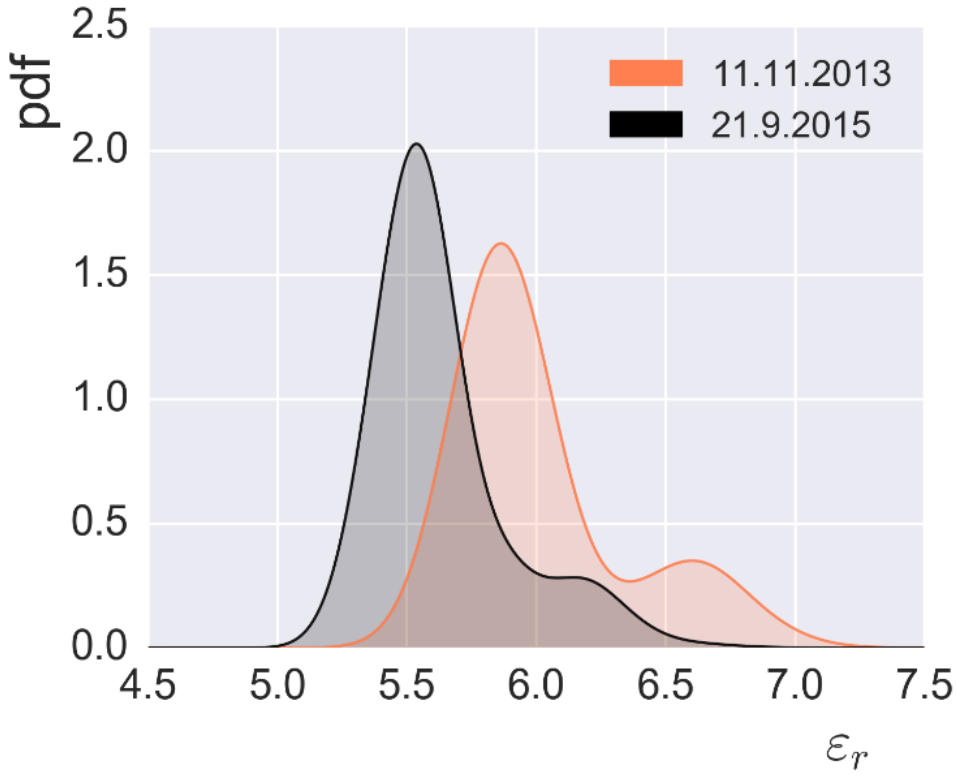

Figure 43: KDE of GPR data measured Vt 12 in 11.11.2013 and 21.9.2015

Table 12: Vt 3 and Vt 12 descriptive statistics

ROAD	ID	Date	Wheel Path	N	mean(ε_r)	std(ε_r)
Vt 3	Before	17.7.2013	Center	4351	7.37	0.38
Vt 3	20 h	20.8.2013	Center	4349	5.10	0.17
Vt 3	6 d	26.8.2013	Center	4351	4.86	0.15
Vt 3	40 d	30.9.2013	Center	4349	5.82	0.22
Vt 3	2 a	21.9.2015	Center	4360	5.54	0.13
Vt 3	Before	17.7.2013	Right	4351	7.22	0.38
Vt 3	20 h	20.8.2013	Right	4350	4.90	0.21
Vt 3	6 d	26.8.2013	Right	4351	4.76	0.14

Vt 3	40 d	30.9.2013	Right	4348	5.91	0.26
Vt 3	2 a	21.9.2015	Right	4360	5.82	0.19
Vt 12	2013 – Total	11.11.2013	Right	3574	6.02	0.34
Vt 12	2013 (0-2800 m)*		Right	2800	5.87	0.14
Vt 12	2013 (3000+ m)*		Right	575	6.65	0.27
Vt 12	2015 – Total	21.9.2015	Right	3580	5.63	0.26
Vt 12	2015 (0-2800 m)*		Right	2830	5.53	0.12
Vt 12	2015 (3000+ m)*		Right	696	6.07	0.22

* (0-2800 m) and (3000+ m) extra IDs describe measurement areas seen in Figure 41 where the permittivity level rises

3.6.1 *Drill core results from permittivity level jump in Vt 12*

The jump in permittivity level close to 2800 m was examined more closely. Six drill cores were extracted from lower and higher permittivity locations, three from each location with 10 meter spacing. Drill cores were then measured with the new cavity resonator method, which produces an accurate estimate for permittivity of the whole drill core. The results are shown below in Table 13.

Table 13: Vt 12 drill core permittivities and dimensions. Locations demonstrate lower (2600) and higher permittivity levels (3000) seen in the permittivity profile in Figure 41. Note that the location of cores is given in the Road Registry numbering system (increasing direction from Pori to Tampere), whereas the GPR measurements run from Tampere to Pori

Location	Layer	Pavement type	Permittivity (mean) (-)	Layer thickness mm	Total asphalt thickness mm
3000-570	**a**	**SMA**	5.6	50	280
3000-570	**b**	**AC**	5.1	45	280
3000-560	**a**	**SMA**	5.6	50	270
3000-560	**b**	**AC**	5.1	35	270
3000-550	**a**	**SMA**	5.6	50	270
3000-550	**b**	**AC**	5.1	40	270
2600-890	**a**	**SMA**	4.9	40	220
2600-890	**b**	**AC**	5.1	30	220
2600-880	**a**	**SMA**	5.2	40	220
2600-880	**b**	**AC**	5.1	40	220
2600-870	**a**	**SMA**	5.4	40	250
2600-870	**b**	**AC**	5.1	45	250

3.6.2 *Conclusions*

Based on the results obtained in 2015 from Vt 3, it can be concluded that at Vt 3, new measurements were comparable to the previous ones. In Vt 12, the increase of permittivity values after 2800 meters was repeatable, suggesting that the increase in permittivity was not due to some temporary circumstance, such as water on the pavement surface or pores. Although the variation of permittivity values in laboratory and GPR measurements correlate, the level of GPR values is higher and cannot be explained only by material properties. This indicates that other factors, such as the structure of pavement, radar calibration or interpretation of signal (filtering) affect the permittivity results obtained.

3.7 GPR results comparison

In this section, GPR permittivity results from different test sites are compared and the influence of averaging is studied. Figure 44 - Figure 46 show sections of permittivities against horizontal scales of 100 m, 10 m and 1 m. The figures show that the permittivities change in a unique manner based on the test site. The following Figure 47-Figure 49 reveal the relationship of averaging the data with binning and the corresponding standard deviation inside the bins.

These results indicate that there are weak positive relationships between standard deviations and mean values, which is also seen in permittivity profile figures shown in previous sections. This means that higher permittivity values have a larger variance. Binned averages and standard deviations show the natural property of averaging where a larger bin size lowers the apparent variance of the sample.

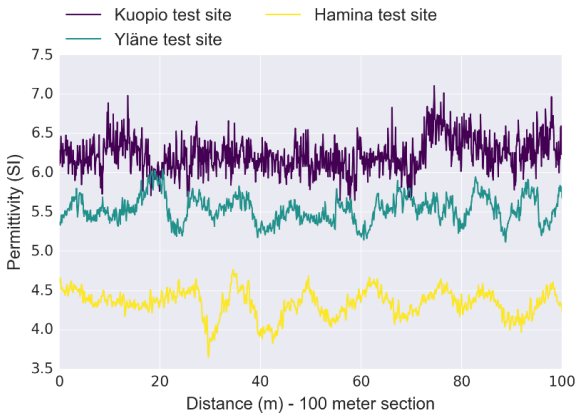

Figure 44: GPR results from different test sites - 100 meter section

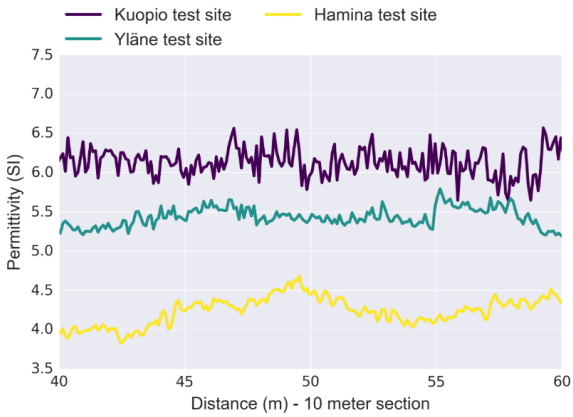

Figure 45: GPR results from different test sites - 10 meter section

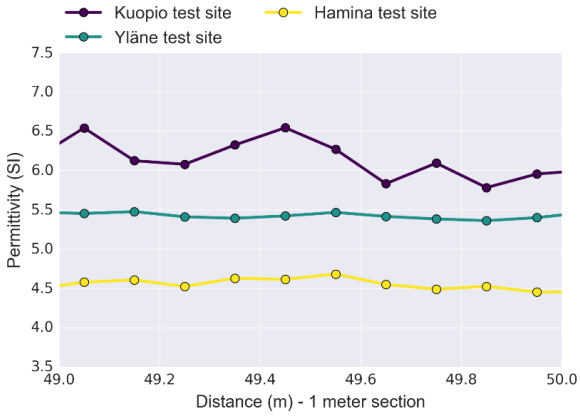

Figure 46: GPR results from different test sites - 1 meter section

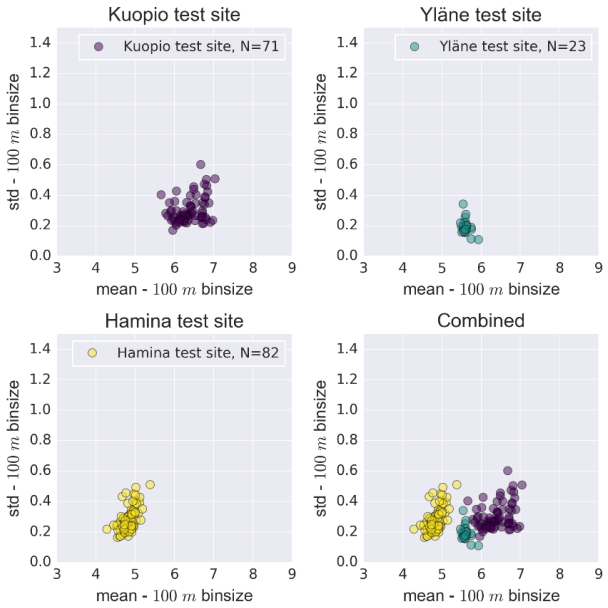

Figure 47: Influence of data binning at different test sites - 100 meter bin size

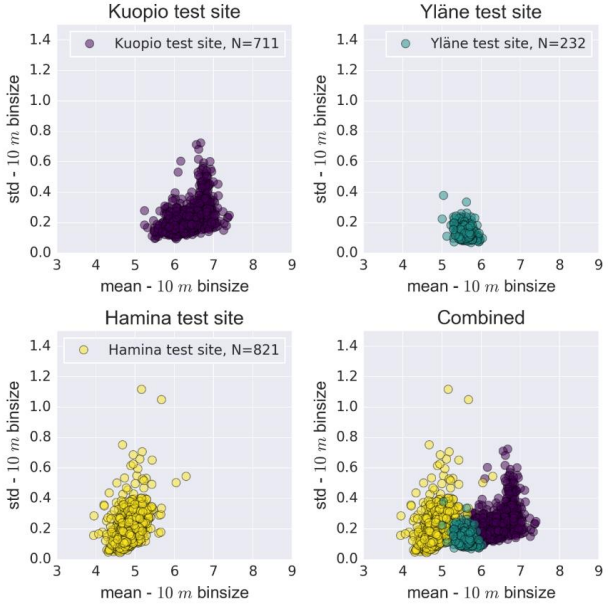

Figure 48: Influence of data binning at different test sites - 10 meter bin size

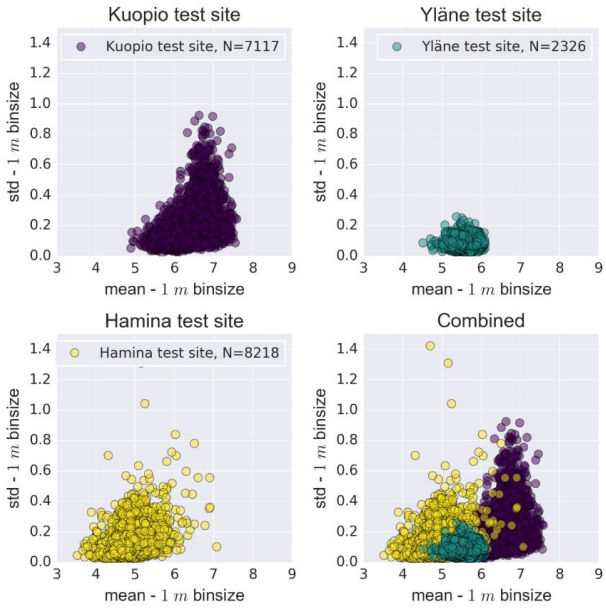

Figure 49: Influence of data binning at different test sites - 1 meter bin size

4 CONCLUDING REMARKS

In this report, we have presented microwave radar and GPR measurements as well as laboratory tests conducted in 2014-2016. The microwave radar was tested in three different construction sites. GPR measurements were obtained, in addition to microwave radar test sites, and in two other test sites. Laboratory tests included traditional density measurements and 7-17 GHz VNA scanning of drill cores obtained from the test sites.

The average of air voids varied among different test sites. However, the range in permittivity values obtained with VNA and microwave radar did not follow the changes in air voids. The range in permittivity values was remarkably large, which indicates that other factors have an influence other than the air void content.

The results indicate no clear correlation between air void content and GRP permittivity measurements. Permittivity is sensitive to the changes in the relative permittivity of aggregates and volume portions of aggregates and bitumen. The relative permittivity of the aggregates determines the base level for permittivity measured with radar or VNA.

A new laboratory measurement method using cavity resonator principle was introduced with promising results. Testing of this new method will be continued.

To summarize, we concluded that error sources in the measured permittivity values ε_r' may be:

- Hardware calibration of radar and steadiness of calibration
- Multiple reflections from layers below (frequency) and pulse width
- Water in the pores (date of measurements)
- Selection of signal maximum amplitude in the analysis (interpretation of data).

Error sources in the calibration procedure for the air void content may include:

- There is water on the pavement and the obtained ε_r' value is larger than the ε_r' for dry pavement (exceeds permittivity of asphalt with refusal density)
- When water is present on the pavement, the PANK calibration equation fails to indicate the large air voids and the variance in the air voids is distorted. Similarly, the average air void content is shown to be lower than it is in reality
- The method for measuring density in the laboratory distorts the real air void content if the sample is thin and porous. This problem has been observed, for example, with very thin Remix-pavements
- The radar measures the absolute air void content, whereas laboratory measurements are relative (mixture-dependent) being, for example, affected differently by the porous surface of the sample

In the course of this research, it has become apparent that a new calibration procedure for the GPR measurements is needed. The aim is to extract core samples from pavement areas with different densities to obtain a local calibration model.

5 REFERENCES

Huuskonen-Snicker, E., Eskelinen, P., Pellinen, T., and Olkkonen M-K. A New Microwave Asphalt Radar Rover for Thin Surface Civil Engineering Applications. Frequenz. Volume 69, Issue 7-8, Pages 377–381, DOI: 10.1515/freq-2015-0034, April 2015

Nevalainen, N. The use of thermal camera for quality assurance of asphalt pavement construction, Master's thesis, Aalto University, 2014.

Olkkonen, M.-K., Eskelinen, P., Huuskonen-Snicker, E., Pellinen, T., and Olmos Martinez, P. A New Microwave Asphalt Radar. *RADAR 2014 (International Radar Conference 2014), 13-17 October, Lille, France.*

Pellinen, T., Eskelinen, P., Huuskonen-Snicker, E., Hartikainen, A. Assessment of air void content of asphalt using dielectric constant measurements by GPR and with VNA. Aalto University publication series SCIENCE + TECHNOLOGY 9/2015. http://urn.fi/URN:ISBN:978-952-60-6288-4

Scott, D.W. On Optimal Data-Based Histograms. Oxford University Press, 1979

This research has been conducted in collaboration with Liikennevirasto (Finnish Transport Agency).

Aalto-ST 8/2016

Finnish Transport Agency

ISBN 978-952-60-6879-4 (pdf)
ISSN-L 1799-4896
ISSN 1799-4896 (printed)
ISSN 1799-490X (pdf)

Aalto University
School of Engineering
Department of Civil Engineering
www.aalto.fi

BUSINESS + ECONOMY

ART + DESIGN + ARCHITECTURE

SCIENCE + TECHNOLOGY

CROSSOVER

DOCTORAL DISSERTATIONS